Science of the Total Environment 923 (2024) 171374

Contents lists available at ScienceDirect

Science of the Total Environment

journal homepage: www.elsevier.com/locate/scitotenv

Effect of Ba(II), Eu(III), and U(VI) on rat NRK-52E and human HEK-293 kidney cells *in vitro*

Christian Senwitz [a,b,1], Daniel Butscher [c,1], Linus Holtmann [d], Manja Vogel [e], Robin Steudtner [c], Björn Drobot [c], Thorsten Stumpf [a,c], Astrid Barkleit [c], Anne Heller [a,b,*]

[a] Technische Universität Dresden, Faculty of Chemistry, Institute of Analytical Chemistry, Professorship of Radiochemistry/Radioecology, 01062 Dresden, Germany
[b] Technische Universität Dresden, SG 4.6 Radiation Protection, Central Radionuclide Laboratory, 01062 Dresden, Germany
[c] Helmholtz-Zentrum Dresden-Rossendorf, Institute of Resource Ecology, 01328 Dresden, Germany
[d] Leibniz Universität Hannover, Institute of Radioecology and Radiation Protection, 30419 Hannover, Germany
[e] VKTA – Strahlenschutz, Analytik & Entsorgung Rossendorf e.V, 01328 Dresden, Germany

HIGHLIGHTS

- Combination of *in vitro* toxicological bioassays and sophisticated spectroscopic methods.
- Eu(III)/U(VI) cytotoxicity correlates with cellular uptake, concentration, and exposure time.
- Ba(II) is not cytotoxic up to 1 mM and cellular uptake is very low independent from time.
- Cellular Eu(III) and U(VI) are dominantly bound to phosphatic binding motifs.
- First-time characterization of intracellular Eu(III) in kidney cells by chemical microscopy.

GRAPHICAL ABSTRACT

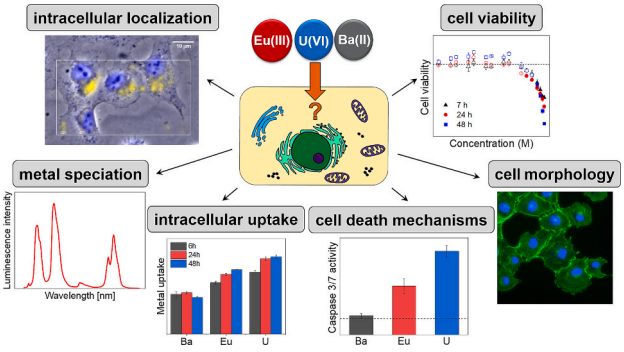

ARTICLE INFO

Editor: Daqiang Yin

Keywords:
Cytotoxicity
Radionuclides
Kidney cells
Heavy metal speciation
TRLFS
Chemical microscopy

ABSTRACT

Heavy metals pose a potential health risk to humans when they enter the organism. Renal excretion is one of the elimination pathways and, therefore, investigations with kidney cells are of particular interest. In the present study, the effects of Ba(II), Eu(III), and U(VI) on rat and human renal cells were investigated *in vitro*. A combination of microscopic, biochemical, analytical, and spectroscopic methods was used to assess cell viability, cell death mechanisms, and intracellular metal uptake of exposed cells as well as metal speciation in cell culture medium and inside cells.

For Eu(III) and U(VI), cytotoxicity and intracellular uptake are positively correlated and depend on concentration and exposure time. An enhanced apoptosis occurs upon Eu(III) exposure whereas U(VI) exposure leads to enhanced apoptosis and (secondary) necrosis. In contrast to that, Ba(II) exhibits no cytotoxic effect at all and its intracellular uptake is time-independently very low. In general, both cell lines give similar results with rat cells being more sensitive than human cells.

* Corresponding author at: Technische Universität Dresden, Faculty of Chemistry, Institute of Analytical Chemistry, Professorship of Radiochemistry/Radioecology, 01062 Dresden, Germany.
E-mail address: a.heller@tu-dresden.de (A. Heller).
[1] These authors contributed equally to this work.

https://doi.org/10.1016/j.scitotenv.2024.171374
Received 20 December 2023; Received in revised form 27 February 2024; Accepted 27 February 2024
Available online 2 March 2024
0048-9697/© 2024 The Authors. Published by Elsevier B.V. This is an open access article under the CC BY license (http://creativecommons.org/licenses/by/4.0/).

The dominant binding motifs of Eu(III) in cell culture medium as well as cell suspensions are (organo-) phosphate groups. Additionally, a protein complex is formed in medium at low Eu(III) concentration. In contrast, U(VI) forms a carbonate complex in cell culture medium as well as each one phosphate and carbonate complex in cell suspensions. Using chemical microscopy, Eu(III) was localized in granular, vesicular compartments near the nucleus and the intracellular Eu(III) species equals the one in cell suspensions.

Overall, this study contributes to a better understanding of the interactions of Ba(II), Eu(III), and U(VI) on a cellular and molecular level. Since Ba(II) and Eu(III) serve as inactive analogs of the radioactive Ra(II) and Am (III)/Cm(III), the results of this study are also of importance for the health risk assessment of these radionuclides.

1. Introduction

Over the past 60 years, the use of radionuclides (RN) in civilian industry, research, and medicine has increased rapidly. Especially due to mining activities, power plant accidents, leaks in repository systems, or use in cancer diagnostics and therapy, these elements can be released into the environment and, hence, pose a possible health risk to humans (Akbar et al., 2016; Ansoborlo and Adam-Guillermin, 2012; Gudelis and Gorina, 2015; Wollenberg et al., 2021; Zhang et al., 2022). In fact, numerous cases of anthropogenic RN uptake in humans are described in the literature. For instance, elevated concentrations of actinides (An) like uranium, thorium, and plutonium were measured in biological samples of workers employed in mineral processing, radioactive waste treatment, and fuel recycling (Lipsztein et al., 2001; Romanov et al., 2020; Zhang et al., 2022).

RN have no known essential biochemical function in living organisms. Instead, acute or chronic exposure pose several risks due to radio- and chemotoxic effects (Ansoborlo et al., 2006). Incorporation by humans can occur *via* inhalation, ingestion, or wound contact (Ansoborlo and Adam-Guillermin, 2012). Once incorporated, RN coordinate to endogenous macromolecules (*e.g.*, albumin or transferrin) and can be transported *via* the blood stream to different target organs (*e.g.*, kidneys, liver, and bones) where they are deposited and/or excreted (Ansoborlo et al., 2006; Ansoborlo and Adam-Guillermin, 2012). Absorption, transport, and excretion vary strongly between the elements and depend primarily on their oxidation state, initial chemical form, and speciation (*i.e.*, binding to ligands from/in body fluids and compartments) (Ansoborlo et al., 2006). In tissues, RN can, then, interact with a variety of cellular constituents like amino acids, proteins, or nucleic acids and exert different adverse effects by competition for biological binding sites, structural perturbations, or generation of reactive oxygen species (ROS) (Ansoborlo and Adam-Guillermin, 2012). Consequently, several health disorders such as carcinogenesis, pneumonia, tissue fibrosis, or nephrological damage can arise (Fattal et al., 2015). Up to date, many publications regarding RN exposure focus on animal models and phenomenological studies including biokinetic processes and metal distribution patterns within organs *in vivo*. However, toxicological data on the cellular and molecular level is still scarce. Due to the central role of urinary excretion for bi-, tri-, and hexavalent RN in mammals, especially kidney cells are of great interest. In the present *in vitro* study, we investigated interactions of renal cells with the elements Ba(II), Eu(III), and U(VI).

The bivalent heavy metal Ba(II) constitutes the non-radioactive chemical analog for the RN Ra(II). Ba(II) exposure studies with rats and mice revealed induction of severe toxicological damage in mammalian kidney tissue like tubular dilatation, deposition of insoluble salt crystals or toxic nephrosis (Dietz et al., 1992). Genotoxic effects and oxidative impacts by ROS generation are also described in the literature (Elwej et al., 2016). However, to the best of the authors' knowledge, *in vitro* Ba(II) exposure studies of renal cell lines have not been conducted yet and correlations between metal speciation, solubility, and bioassociation are still largely unknown.

Urinary excretion is also described for lanthanides (Ln) like Eu(III) (Leggett et al., 2014), which represents a non-radioactive analog of the An Cm/Am(III). Due to their very similar physicochemical properties, Ln (III) are considered to be suitable substitutes providing a good approximation for data not available for An(III) (Günther et al., 2022; Jessat et al., 2022). However, the only studies examining cytotoxic effects of Eu (III) on rat and human kidney cells were recently conducted by Heller et al. (2021, 2019). These investigations revealed time- and concentration-dependent effects of Ln(III) on both cell viability and morphology. The presence of serum proteins was found to reduce Eu(III) cytotoxicity and to have a great impact on metal speciation and solubility in the cell culture medium. However, further *in vitro* analyses are necessary to establish interdependencies of intracellular Eu(III) speciation, metal uptake, and cytotoxicity in kidney cells. Furthermore, the localization of Eu(III) accumulated inside cells is still pending.

Most research regarding interactions of RN with mammalian kidney cells has been done with the hexavalent An U(VI). Remarkably, 65 % of incorporated U(VI) are eliminated *via* urine within one day but a substantial portion of the element is temporarily retained in the renal tissue (ICRP, 1995). Thus, several U(VI) exposure studies were conducted with rat kidney cells, investigating different toxicological endpoints as well as relationships between metal accumulation and cytotoxicity (Carrière et al., 2004, 2005b, 2006; Milgram et al., 2007; Thiébault et al., 2007). In most of these experiments U(VI) was applied as bicarbonate or citrate and a maximum exposure time of 30 h. It could be shown that the presence of citrate increases intracellular accumulation of U(VI) and leads to a higher cytotoxicity (Carrière et al., 2004; Milgram et al., 2007). Since X-ray absorption spectroscopic studies state predominant formation of U(VI)-bicarbonate species in the cell culture medium, the increased cytotoxicity may not arise from different speciation but from co-transport effects with the counterion (Carrière et al., 2006). On the molecular level, U(VI) causes intrinsic caspase-dependent apoptosis induction from 200 μM and genotoxic effects from 300 μM on (Thiébault et al., 2007). In spite of all the studies done so far, the underlying cell death mechanisms upon renal U(VI) exposure are still under investigation and involvement of recently described cellular processes, such as pyroptosis (Zheng et al., 2022), has to be evaluated. Furthermore, most studies were performed in serum-free minimal essential medium (MEM). Since serum contains multiple essential vitamins and growth factors, removing the serum content of a cell culture medium leads to significant cellular stress. The cell metabolism adopts trying to compensate the lack of serum. This may also lead to a different strength of cellular response to heavy metal exposure. We, therefore, conducted our experiments in serum-supplemented medium. Finally, in contrast to rat cells, human kidney cells are only partly investigated (Cheng et al., 2022; Hao et al., 2014; Prat et al., 2005) and published toxicological data sets of effective concentrations are still incomplete for these cell lines.

In our comparative study, epithelial-like kidney cells of rats (NRK-52E cell line) and embryonal kidney cells of humans (HEK-293 cell line) were exposed to Ba(II), Eu(III), or U(VI) in serum-containing medium for up to 48 h. To ensure comparability of the results, all elements were applied as chloride salts. Since chloride is ubiquitous at elevated concentrations in biological systems, it does not exhibit any toxicological effect and possible co-transport effects with additionally applied anions (*e.g.,* citrate) are avoided. The overall aim was to reveal correlations between cytotoxicity, intracellular metal uptake, and speciation of the used elements. Therefore, biological methods determining toxicological endpoints (*i.e.*, cell viability, apoptosis and necrosis, caspase 3/7

activity, and ROS generation) were combined with physicochemical analyses (luminescence spectroscopy, mass spectrometry, and chemical microscopy) examining speciation and accumulation of the applied metals inside the cells.

2. Material and methods

2.1. Cell culture

Normal rat kidney cells (NRK-52E; (De Larco and Todaro, 1978)) were purchased from the European Collection of Authenticated Cell Cultures (ECACC 87012902; United Kingdom). Human embryonal kidney cells (HEK-293; (Graham et al., 1977)) were derived from Deutsche Sammlung von Mikroorganismen und Zellkulturen (DSMZ; ACC 305; Germany). Both cell lines were cultivated at 37 °C, 95 % relative humidity (rH), and 5 % CO_2 in Dulbecco's Modified Eagle's Medium (DMEM; high glucose with sodium pyruvate; Capricorn Scientific, Germany) supplemented with 10 % (*v*/v) fetal bovine serum (FBS; Biowest, USA), 1 % (v/v) penicilline/streptomycine, and 4 mM glutamine (both purchased from Thermo Fisher Scientific, USA). U(VI) exposure experiments with NRK-52E cells were also conducted in pyruvate-free DMEM (high glucose, Capricorn Scientific, Germany), using the same supplements mentioned above.

All cells were cultivated until 90 % confluence in 75 cm^2 cell culture flasks (CELLSTAR®, greiner bio-one, Germany). Passages 5–14 (NRK-52E) and 12–21 (HEK-293) were used for all experiments.

2.2. Chemicals

Ba(II) and Eu(III) were applied as chlorid salts ($BaCl_2 \cdot 6\ H_2O$, $EuCl_3 \cdot 6\ H_2O$; > 99 % trace metal basis; Sigma Aldrich Chemie GmbH, Germany). U(VI) was purchased as $UO_2(NO_3)_2 \cdot 6\ H_2O$ from Chemapol (Czech Republic). To obtain a U(VI) chloride solution, a 10 % U(VI) nitrate solution was first converted to $UO_4 \cdot 4\ H_2O$ by adding 30 % H_2O_2 (1.5 mL/g U(VI)). The U(VI) peroxide was, then, transformed at 220 °C for 6 h to UO_3, which was dissolved in 0.1 M HCl.

For all metals, stock solutions of each 10 mM were prepared in double distilled water and sterile filtered through 0.20 μm filters (Whatman®, GE Healthcare Life Sciences, Germany) before use.

For cell viability determination, 50 mg/mL XTT (2,3-bis-(2-methoxy-4-nitro-5-sulfophenyl)-2H-tetrazolium-5-carboxanilide) in cell culture medium and 3 mg/mL PMS (5-methylphenazinium methyl sulfate; both purchased from SERVA Electrophoresis GmbH, Germany) in phosphate buffered saline (PBS) were used.

PBS was prepared from 2.7 mM KCl, 137 mM NaCl (both ≥ 99.0 %, Fisher Scientific, United Kingdom), 10 mM $Na_2HPO_4 \cdot 2\ H_2O$, and 1.8 mM KH_2PO_4 (both ≥ 99.0 %, VWR Chemicals, USA).

Cytochemical staining of cells was carried out using the following stock solutions: 4 % (*v*/v) paraformaldehyde (96 %; Acros Organics, Belgium) in PBS, 1 % (v/v) bovine serum albumin (BSA; AppliChem GmbH, Germany) in PBS, 10 % (v/v) Triton X-100 (Sigma-Aldrich Chemie GmbH, Germany) in PBS, 5 mg/mL DAPI (4′,6-diamidin-2-phenylindol; Santa Cruz Biotechnology Inc., USA) in water, Phalloidin-iFluor™ 488 Conjugate (AAT Bioquest Inc., USA) in DMSO according to the manufacturer's protocol, and Mowiol 4–88 (Carl Roth GmbH + Co. KG, Germany) according to the manufacturer's protocol.

2.3. Determination of cell viability after metal exposure

Cytotoxicity experiments were carried out in 96-well cell culture plates (TPP Techno Plastic Products AG, Switzerland). Sub-cultured cells were seeded at different cell densities depending on the cell line and metal exposure time: $3{\cdot}10^4$ (NRK-52E) or $1{\cdot}10^5$ cells/mL (HEK-293) were seeded for 7 h experiments, $2{\cdot}10^4$ (NRK-52E) or $5{\cdot}10^4$ cells/mL (HEK-293) for 24 h and $1{\cdot}10^4$ (NRK-52E) or $2{\cdot}10^4$ cells/mL (HEK 293) for 48 h cytotoxicity experiments, respectively. Each well contained 100 μL of cell suspension. The use of different cell densities ensured sub-confluence of seeded cells in all plates after the respective exposure time. Prior to exposure, the cells were incubated for 24 h to adhere. Afterwards, the cell culture medium was replaced by 100 μL fresh medium containing $1{\cdot}10^{-9}$ to $3{\cdot}10^{-3}$ M heavy metal (Ba(II), Eu(III), or U(VI)) and the cells were exposed for 7, 24, or 48 h, respectively.

Cell viability after metal exposure was determined with the XTT assay, measuring the mitochondrial activity of the cells (Scudiero et al., 1988). In this assay, the tetrazolium salt XTT is reduced to a colored formazan dye, which can be detected by absorbance measurements with a microplate reader (Cytation 5, Agilent Technologies, USA) at 492 nm. The reaction is mediated by the electron donor PMS. The assay also included untreated and Zn(II) treated ($5{\cdot}10^{-5}$ M) cells as negative and positive control, respectively. $ZnCl_2$ (≥ 98.0 %, VWR Chemicals, USA) was used as a positive control due to its known cytotoxic effect (Heller et al., 2019, 2021; Plum et al., 2010). Cell viability was determined in relation to the untreated cells (100 % viability) of each plate. For each metal (Ba(II), Eu(III), U(VI)) and exposure time (7, 24, or 48 h), at least, four independent experiments were conducted (biological replicates) with all samples, blanks, and controls in quadruplicates (technical replicates).

2.4. Cytochemical staining and fluorescence microscopy

Cytochemical staining was conducted using 8-chamber cell culture slides (Falcon®, Corning, USA) with a glass cover slip. Sub-cultured NRK-52E cells were seeded at a density of $2{\cdot}10^4$ cells/mL (100 μL/well) and incubated for 24 h to attach. After that, cells were exposed to $1{\cdot}10^{-3}$ M Ba(II), Eu(III), or U(VI) like in the cell viability studies (see Section 2.3). Additionally, each slide contained negative (untreated cells) and positive controls (cells treated with $5{\cdot}10^{-5}$ M Zn (II)). After 48 h, the cells were fixed on the cell culture slides with 4 % (*v*/v) paraformaldehyde in PBS and permeabilized with 0.1 % Triton X-100. Staining of the cytoskeleton was performed using Phalloidin-iFluor™ 488 Conjugate in 1 % BSA. Mowiol containing the DNA dye DAPI was applied as mounting medium. The slides were, finally, dried at room temperature overnight and, then, stored at 4 °C in the dark.

Fluorescence microscopic images were taken with a cell imaging multimode reader (Cytation 5, Agilent Technologies, USA) using a 20× objective and the respecting GFP and DAPI filter channels.

2.5. Bioassays

The following section describes the conducted bioassays for the determination of apoptosis and necrosis levels, caspase 3/7 activity, and ROS production upon metal exposure.

All assays were carried out with sub-cultured NRK-52E cells in black 96-well cell culture plates (CELLSTAR®, greiner bio-one, Germany) and included cell exposure to $1{\cdot}10^{-3}$ M Ba(II), Eu(III) or U(VI) in comparison to untreated control cells. The cells were seeded at a cell density of $1.5{\cdot}10^3$ cells/well and incubated for 24 h prior to the experiments to adhere.

2.5.1. Apoptosis and necrosis differentiation

The non-lytic RealTime-Glo™ Annexin V Apoptosis and Necrosis Assay (Promega Corporation, USA) was used to differentiate between both cell death mechanisms upon exposure to 10^{-3} M Ba(II), Eu(III), or U(VI) in a kinetic approach. The assay contains annexin V luciferase fusion protein, which binds to phosphatidylserine exposed on the inner membrane leaflets of apoptotic cells (luminescence signal), as well as a DNA-binding dye, which enters necrotic cells with disturbed membrane integrity (fluorescence signal, 485 nm_{Ex}/525 nm_{Em}). The assay was applied according to the manufacturer's protocol.

Metal solutions and assay reagents were added to the cells simultaneously at t_0 and the plates were incubated for 48 h at 37 °C. $5{\cdot}10^{-4}$ M Zn(II) was used as a positive control. The luminescence and fluorescence

signals were measured in real-time after 1, 3, 6, 24, 30, and 48 h with a microplate reader (Cytation 5, Agilent Technologies, USA) from the same wells. Both luminescence and fluorescence signals of metal exposed cells were correlated to untreated control cells. For each metal (Ba(II), Eu(III), U(VI)), at least three independent experiments were conducted with all samples in quadruplicates.

2.5.2. Caspase 3/7 activity

Caspases 3 and 7 are proteolytic key effectors that are involved in signal cascades leading to apoptosis (Fink and Cookson, 2005). Their activity was measured with the Apo-ONE® Homogeneous Caspase-3/7 Assay (Promega Corporation, USA), consisting of a bifunctional cell lysis/activity buffer and a profluorescent substrate, which gets fluorescent upon sequential cleavage by caspase 3/7 (499 nm_{Ex}/521 nm_{Em}). The assay was applied according to the manufacturer's protocol.

The seeded cells were exposed to 10^{-3} M Ba(II), Eu(III), or U(VI) for 24 h at 37 °C. 100 nM staurosporine, a typical apoptosis inducer, was used as a positive control. After the incubation, the caspase 3/7 assay was added to the wells and the plates were kept at room temperature for 2 h. Fluorescence signals were measured with a microplate reader (Cytation 5, Agilent Technologies, USA). Signals of exposed cells were correlated to untreated control cells. For each metal (Ba(II), Eu(III), U (VI)) four independent experiments were conducted with all samples in quadruplicates.

2.5.3. Reactive oxygen species production

The cellular ROS levels upon metal exposure were determined using the ROS-Glo™ H_2O_2 Assay (Promega Corporation, USA). H_2O_2 has a long intracellular half-life and plays a central role in ROS metabolism (Alfadda and Sallam, 2012). Changes in H_2O_2 levels can reflect general changes of ROS levels in cells (Alfadda and Sallam, 2012). The assay uses a prosubstrate, which reacts with H_2O_2 and D-cysteine to luciferin. The latter reacts with a luciferase to generate a luminescence signal. The assay was applied according to the manufacturer's protocol.

In brief, cells were exposed to 10^{-3} M Ba(II), Eu(III), or U(VI) and incubated at 37 °C for 24 h. 100 μM menadione, a known ROS inducer, was used as a positive control. 6 h prior to the measurements, the prosubstrate was added to the cells. At the end of the exposure time, D-cysteine and luciferase were added and the resulting luminescence signals were measured with a microplate reader (Cytation 5, Agilent Technologies, USA). H_2O_2 levels of exposed cells were correlated to untreated control cells. For each metal (Ba(II), Eu(III), U(VI)), four independent experiments were conducted with all samples in quadruplicates.

2.6. Intracellular metal uptake

To investigate the uptake of the metal ions into the cells, the subcultured cells were seeded with 3 mL medium per well in 6-well cell culture plates (TPP Techno Plastic Products AG, Switzerland) and incubated for 24 h at 37 °C, 95 % rH and 5 % CO_2 to adhere. The cell densities were varied according to cell line and metal exposure time as follows: for NRK-52E cells, $1{\cdot}10^5$ cells/mL were used for 6 h, $5{\cdot}10^4$ cells/mL for 24 h, and $3{\cdot}10^4$ cells/mL for 48 h of metal exposure. In contrast, HEK-293 cells were seeded at $3{\cdot}10^5$ cells/mL for 6 h, $1.5{\cdot}10^5$ cells/mL for 24 h, and $5{\cdot}10^4$ cells/mL for 48 h metal exposure. After 24 h, the medium was replaced with 3 mL of fresh medium containing 10^{-5} or 10^{-3} M metal ions and the cells were exposed for 6, 24, or 48 h, respectively. After exposure, the cells were processed based on a previously published protocol (Sachs et al., 2015). In brief, the metal solution was removed and the cells were washed three times with 1 mL 0.9 % NaCl solution. To detach the cells from the wells and remove the metal bound/sorbed onto the cell surface, the exposed cells were treated for 5 min with 0.55 mL of trypsin/EDTA (0.05 %/0.02 %) dissolved in PBS. Trypsinization was, then, stopped by adding 0.45 mL of fresh complete cell culture medium. Since in some bacterial species only a small proportion of U(VI) can be extracted from the biomass with EDTA (Panak et al., 1999), additional experiments were carried out with U (VI)-exposed cells using editronic acid (HEDP, $5{\cdot}10^{-4}$ M) in PBS instead of trypsin/EDTA. HEDP is considered a potential U(VI) decorporation agent, which shows a good washing effect (Carrière et al., 2005b). A small aliquot of each solution was taken for cell counting (counting chamber, Neubauer, Germany). The remaining suspension was centrifuged at 200 ×*g* for 5 min (Eppendorf, MiniSpin centrifuge, Germany) and the supernatant was carefully removed. Then, the resulting cell pellet was suspended in 0.5 mL double distilled water. For cell lysis, a fivefold freeze-thaw lysis was carried out. To separate the cell debris, centrifugation (15 min, 4700 ×*g*) was performed, and the supernatant was collected for the determination of the metal concentration in the cells by ICP-MS. For each metal and exposure time, three independent experiments were performed with all samples in duplicate.

2.7. Solubility in cell culture medium

The solubility of Ba(II), Eu(III), and U(VI) in cell culture medium was investigated according to a previously published method (Carrière et al., 2005a; Heller et al., 2019, 2021). In brief, metal concentrations of 10^{-5}–10^{-3} M were adjusted in cell culture medium in 24-well cell culture plates (TPP Techno Plastic Products AG, Switzerland) and incubated at 37 °C, 95 % rH, and 5 % CO_2 for 24 or 48 h, respectively. The Eu (III) and U(VI) solutions were, then, filtered through a 0.22 μm sterile filter with a polyethersulfone membrane (Whatman®, GE Healthcare Life Sciences, Germany). Since sorption processes are likely to occur on the filter membrane during filtration of Ba(II), the solutions were instead subjected to ultracentrifugation (Optima XPN-80, Beckman Coulter, Krefeld, Germany) at 214,200 × g for 30 min. The filtrates and the centrifugates were analyzed by inductively coupled plasma mass spectrometry (ICP-MS) using either a NexION 350X (1300 W; Perkin Elmer, Germany) or an iCap RQ (1550 W; Thermo Fisher Scientific, Germany). The metal concentration measured corresponds to the dissolved fraction. Each sample was conducted as duplicates. Thermodynamic modelling of the speciation and solubility of Ba(II) in inorganic cell culture medium was performed using PhreePlot (Kinniburgh and Cooper, 2011) with the ThermoChimie v11 database (Giffaut et al., 2014). PhreePlot contains an embedded version of PhreeqC version 3.7 (Parkhurst and Appelo, 2013).

2.8. Time-resolved laser-induced fluorescence spectroscopy (TRLFS)

2.8.1. Sample preparation

TRLFS spectroscopy was used to study the speciation of Eu(III) and U (VI) in the cells as well as in the cell culture media. 10 mL of the subcultured cells (NRK-52E: $5{\cdot}10^4$ cells/mL; HEK-293: $1{\cdot}10^5$ cells/mL) were seeded in 75 cm^2 cell culture flasks (CELLSTAR®, Greiner bio-one, Germany). After 24 h, the cell culture medium was substituted with 10 mL of fresh medium containing 10^{-5} or 10^{-3} M metal solution (Eu(III) or U(VI), respectively), and the cells were incubated for 7 (U(VI) only), 24, or 48 h. Then, the metal containing supernatant was carefully removed and filled directly into cuvettes (Eu(III): VWR, Hellma quartz glass cuvette, 117.200F-QS; U(VI): Roth, Rotilabo disposable UV cuvettes, XK26.1). After the cells were washed three times with 0.9 % NaCl (pH 7), they were detached from the wells using a cell scraper (rotatable blade 12 mm, Techno Plastic Products AG, Switzerland). 1.5 mL of the cell suspension (0.9 % NaCl + cells) were filled into cuvettes for measurement. Cell-free culture medium containing Eu(III) or U(VI) was also examined by TRLFS. The same concentrations as well as exposure times as for the cell samples were used. For U(VI), additional samples were collected 3 h after exposure. The U(VI)-containing cell culture media were frozen in liquid nitrogen and stored at −20 °C until measurement. All other samples were measured immediately after preparation.

2.8.2. TRLFS setup

For the measurement of the Eu(III) samples, a diode pumped solid state laser (Ekspla, Vilnius, Lithuania, NT230, 1.3 mJ/pulse) with a pulse width of 5 ns and an excitation wavelength of 394 nm was used for excitation at room temperature. The emitted light was guided by a light guide to the spectrograph (Andor, SR-303i-A, Andor, Oxford Instruments, Abingdon), which is equipped with an ICCD camera (Andor iStar, DH320T-18U-63) for recording the spectra. The following parameters were used: 300 μm input slit, gate width 0.5 ms, gain 4095, 0.0123 s exposure time, 200 accumulations. To record time-dependent luminescence spectra, the delay time between laser pulse and camera control was sampled in 30 dynamic time intervals between 1 and 2000 μs.

For U(VI) TRLFS, the system consists of a Nd:YAG laser (Inlite series, Continuum, San Jose, California, USA) with a laser energy of 3 mJ and a pulse width of 5 to 8 ns, with the excitation wavelength set to 266 nm by frequency quadruplication. The spectrometer applied was an iHR 550 (slit width 200 μm, Horiba, Oberursel, Germany) equipped with an ICCD camera (Horiba, Oberursel, Germany) cooled to 4 °C. The spectrometer was calibrated to 546.07 nm with a mercury-argon lamp (Hg and Ar lines from 253 to 922 nm, Ocean Optics, Dunedin, Florida, USA). The spectra were recorded in the range from 370 to 670 nm with a puls width of 2000 μs at a working frequency of 20 Hz and, then, baseline corrected using LabSpec 5 (Horiba, Oberursel, Germany). Each spectrum was averaged over 100–200 scans. The dynamic step size was defined for the time-resolved measurements in the range from 0.1 to 12,502 μs. All U(VI) measurements were performed at low temperatures (−120 °C) by cooling with constant N_2 gas flow to minimize possible quenching effects of chloride and organic components (Steudtner et al., 2010).

2.9. Mass spectrometry with electrospray ionization (ESI-MS)

Mass spectrometry was used to study the speciation of Ba(II) in the cell-free culture medium and its components. ESI-MS was conducted using an ESI-Source (Thermo Scientific Nanospray Flex Ion Source) coupled to an Orbitrap mass spectrometer (Thermo Scientific Orbitrap Elite). 10 μL of cell culture medium labelled with Ba(II) (final concentration 10^{-5} or 10^{-3} M) were transferred into the nanospray emitters (Proxeon Medium NanoES spray capillaries). Mass spectra were acquired in both positive and negative ion mode in the range of *m/z* 60–1000 and 100–1000, respectively. All measurements were taken at a capillary temperature of 275 °C and with a mass resolution (FWHM) of 120,000 at m/z 400.

2.10. Chemical microscopy

Chemical microscopy was performed to investigate the speciation and spatial distribution of Eu(III) within exposed renal cells. Prior to the analysis, sub-cultured NRK-52E cells were seeded at a density of $2{\cdot}10^4$ cells/mL (100 μL/well) in 8-chamber culture slides (Falcon®, Corning, USA) and incubated for 24 h at 37 °C to attach. Following exposure to $1{\cdot}10^{-4}$ M or $5{\cdot}10^{-4}$ M Eu(III) for further 24 h, the cells were fixed with 4 % (*v*/v) paraformaldehyde in 0.9 % (*w*/*v*) NaCl on the culture slides and permeabilized with 0.1 % Triton X-100. Mowiol with DAPI was applied as a mounting medium. The slides were, finally, dried at room temperature overnight and stored at 4 °C in the dark.

Luminescence spectroscopic mapping of intracellular Eu(III) species was performed using a Raman microscope (LabRAM system, Horiba Jobin Yvon, Lyon, France), equipped with a 532 nm laser for excitation. The according proof of concept was recently described by Vogel et al. (2021).

Selected areas of exposed cells (region of interest - ROI) were spectroscopically mapped using the following parameters: 60× objective, 300 μm pinhole, 200 μm slit width, 300 lines mm^{-1} grating and up to 45 s exposure time. The luminescence light was collected in the 560–725 nm wavelength range. Data acquisition was performed with Labspec 5 software (Horiba Jobin Yvon) followed by data deconvolution by means of non-negative iterative factor analyses (NIFA) as described in Vogel et al. (2021).

Additional phase contrast and fluorescence micrographs were taken on an Olympus BX-61 microscope (Olympus, Hamburg, Germany). To relocate the ROI mapped by means of chemical microscopy on other microscopes, an England finder (Graticules optics, Tonbridge, United Kingdom) was used. Respective cells were imaged through the DAPI filter channel and phase contrast mode. Finally, an overlay of the luminescence spectroscopic mapping, the phase contrast, and the DAPI filter images was created using the ImageJ/Fiji plug-in Correlia (Rohde et al., 2020) to determine the spatial distribution of the Eu(III) species within the cells.

2.11. Data analysis and statistics

2.11.1. Cell culture experiments

All cell culture experiments were evaluated for outliers using the Grubb's test on each technical quadruplicate (Grubbs, 1969). Cell viabilities were calculated as means ± standard deviation (SD) in relation to the untreated control cells (equaling 100 %). Statistical significances were identified by one-way ANOVA including Tukey and Bonferoni *post hoc* test ($p < 0.05$; 95 % confidence) using Origin (OriginPro 2020b, OriginLab Corporation, USA). For EC_{50} calculation, all dose-response curves of one metal for one constant exposure time were fitted altogether using Origin and the following equation:

$$y = \frac{A_1 - A_2}{1 + \left(\frac{x}{x_0}\right)^p} + A_2 \quad (1)$$

with y: cell viability after metal exposure; A_1: initial/highest cell viability; A_2: lowest/final cell viability (fixed to 0 %); x: metal concentration; x_0: center of the curve; p: power. EC_{50} ± standard error of the mean (SEM) equals x_0.

2.11.2. Speciation studies

Data analysis of mass spectra was performed using Thermo Scientific FreeStyle and an in-house software named MARI (Stadler et al., 2023). Species of interest were identified based on their theoretical mass-to-charge ratio and specific isotopic pattern. Mass accuracy was 5 ppm or better for all species identified.

TRLFS data were analyzed with parallel factor analysis (PARAFAC) as described elsewhere (Drobot et al., 2015) using MATLAB 2020b software (The Mathworks Corporation, Natick, MA) and Origin (OriginPro 2020b, OriginLab Corporation, USA).

The fluorescence spectra of Eu(III) were normalized to the $^5D_0 \rightarrow {}^7F_1$ transition. An important parameter for the comparison of different Eu(III) species is the relative peak intensity (*I*) ratio ($R_{E/M}$), which was calculated from the electric dipole transition $^5D_0 \rightarrow {}^7F_2$ and the magnetic dipole transition $^5D_0 \rightarrow {}^7F_1$ (Eq. (2)).

$$R_{E/M} = \frac{I\left({}^5D_0 \rightarrow {}^7F_2\right)}{I\left({}^5D_0 \rightarrow {}^7F_1\right)} \quad (2)$$

The equation of Kimura and Kato (Kimura and Kato, 1998) was used to calculate the number of Eu(III)-coordinated water molecules (N_{H_2O}):

$$N_{H_2O} = \frac{1.05}{\tau} - 0.44 \quad (3)$$

with τ: luminescence emission lifetime in ms.

3. Results and discussion

3.1. Cell viability of kidney cells after barium(II), europium(III), and uranium(VI) exposure

The viability of rat (NRK-52E) and human (HEK-293) kidney cells exposed to Ba(II), Eu(III), or U(VI) strongly depends on the used metal, the exposure time, and the applied metal concentration. Table 1 summarizes the cell viability at the highest metal concentration applied (10^{-3} M) and the EC_{50} values for each exposure time, which were derived from the dose-response curves depicted in Fig. 1.

Ba(II) exhibits no significant time- or concentration-dependent effect on the cell viability of NRK-52E and HEK-293 cells after 48 h within the used concentration range. Even at the highest concentration, cell viability of Ba(II) exposed cells equals that of unexposed control cells for both cell lines (see Table 1). Hence, EC_{50} values for Ba(II) cannot be calculated and result in $EC_{50} >> 1000$ μM (see Table 1). Due to this, experiments with shorter exposure times were omitted.

In contrast to Ba(II), Eu(III) exhibits a measurable effect onto the viability of NRK-52E and HEK-293 cells after exposure for 24 and 48 h. After 24 h, cell viability of both cell lines is unaffected up to $8{\cdot}10^{-4}$ M Eu (III). However, significant effects arise after exposure to 10^{-3} M (see Fig. 1). After 48 h, the cytotoxic effects become even more pronounced. Concentrations above $6{\cdot}10^{-4}$ M Eu(III) cause a significant loss of cell viability in NRK-52E. In contrast, the HEK-293 cell viability remains unaffected up to $8{\cdot}10^{-4}$ M. Short-time Eu(III) exposure for 7 h has no significant impact on NRK-52E or HEK-293 cell viability at all (see Table 1). The results indicate time and concentration dependence of Eu (III) cytotoxicity for both cell lines. The EC_{50} value could only be calculated for 48 h exposure time and is comparable for both NRK-52E and HEK-293 cells.

Of all metals applied, U(VI) reveals the highest cytotoxicity to the kidney cells. In fact, it is the only element showing significant effects after short-time exposure for 7 h with first significant reduction of cell viability at $4{\cdot}10^{-4}$ M U(VI) in both cell lines (see Fig. 1). Therefore, in case of U(VI), an EC_{50} value can be stated even for short-time exposure of 7 h (see Table 1). Prolonged exposure time enhances U(VI) cytotoxicity. After 24 and 48 h, first significant effects arise upon treatment with 10^{-4} M and $4{\cdot}10^{-4}$ M U(VI) for NRK-52E and HEK-293 cells, respectively. Hence, the resulting EC_{50} values are the lowest of all three heavy metals.

In the present study, all cell exposure experiments were conducted in DMEM cell culture medium with sodium pyruvate (see ESI for media composition, Table S1). Since pyruvate serves as a secondary C-source and thus enhances cell growth, a promoting effect on metal cytotoxicity was suspected. Regarding U(VI), we therefore also conducted 24 and 48 h exposure experiments with NRK-52E in pyruvate-free DMEM under the same conditions (*i.e.*, concentration range and cell cultivation parameters). Although the EC_{50} value without pyruvate is slightly higher after 24 h (see Table 1), the differences between both media are not significant (see also ESI, Fig. S1 and Table S2). Regarding Eu(III), our calculated EC_{50} values for 48 h exposure experiments fit very well to the results of Heller et al. (2019), who used DMEM without pyruvate and reported 1070 ± 39 μM for NRK-52E cells and 1020 ± 10 μM for HEK-293 cells under the same conditions. Hence, these comparisons indicate overall independence of Eu(III) and U(VI) cytotoxicity from pyruvate under the selected conditions.

Table 2 summarizes EC_{50} values of various heavy metals after exposure of NRK-52E and HEK-293 for 24 h from literature. Some of the listed reference data is based on experiments in serum-free cell culture medium. Therefore, these values are not directly comparable with our results but serve as a demonstration of distinct metal toxicity levels.

Although Ba(II) constitutes a known environmental toxicological agent and severe renal damage due to high $BaCl_2$ doses is described in the literature (Ananda et al., 2013; Dietz et al., 1992; Mohammed and Ismail, 2017; Wetherill et al., 1981), to the best of the authors knowledge, EC_{50} values for single kidney cell lines are not available in the literature. In humans, the overall estimated median lethal dose (LD_{50}) of $BaCl_2$ is around 1 g for a 70 kg person (Machata, 1988). In rats, first renal effects occur at 60 mg/kg/day of Ba(II) (Dallas and Williams, 2001) and severe treatment related kidney lesions in rodents could be observed at high oral concentrations of $1.6{\cdot}10^{-2}$ M $BaCl_2$ (Dietz et al., 1992). Our *in vitro* study complements the existing *in vivo* data, indicating no cytotoxic effects after direct exposure to 10^{-3} M Ba(II). Because of no effects even after 48 h, the EC_{50} for 24 h exposure is estimated to be much higher than 1000 μM (see Table 2).

For Eu(III), the EC_{50} values are higher than those of other Ln like La (III), Yb(III), or Ce(III) (see Table 2). However, this is only valid in the presence of serum proteins. Studies with serum-free media reveal a higher Eu(III) cytotoxicity and intracellular accumulation upon exposure due to the formation of phosphate precipitates (Heller et al., 2021; Sachs et al., 2015).

U(VI) cytotoxicity roughly ranges between Ln like Eu(III) or Yb(III) and potent cytotoxic heavy metals like Zn(II) or Cd(II) (see Table 2). The toxicological differences between the various U(VI) salts (carbonate, nitrate, acetate, chloride, citrate; see Table 2) possibly arise (in part) from the different media compositions used in the published studies (MEM *vs.* DMEM; serum-free *vs.* 10 % serum), which could influence intracellular U(VI) accumulation and the overall metal metabolism. Especially the serum content is known to be crucial for metal solubility and cytotoxicity (Domínguez et al., 2002; Haase et al., 2015; Heller et al., 2021). Another possibility could be an altered mode of action due to the presence of the respective counter ion. In the case of citrate, it was shown that its presence does not influence U(VI) speciation in the medium but enhances intracellular U(VI) accumulation and thus leads to higher cytotoxicity values (Carrière et al., 2006). Similar effects are conceivable for other anions, *e.g.*, phosphate or bicarbonate, which can be co-transported or, inversely, anti-transported with U(VI) complexes and, therefore, influence intracellular metal uptake (Carrière et al., 2005b).

Especially regarding U(VI) exposure, NRK-52E cells seem to be slightly more susceptible than HEK-293 cells, exhibiting lower overall viability values and higher EC_{50} values after 7 and 24 h, respectively (see Table 1). Higher vulnerability of NRK-52E cells compared to HEK-293 cells is also described in the literature for Ce and Yb exposure (Heller et al., 2019). One reason may be differences in the underlying cytotoxic

Table 1
Comparison of EC_{50} values and cell viability after exposure of kidney cells to Ba(II), Eu(III), and U(VI).

		7 h exposure		24 h exposure		48 h exposure	
Metal	Cell line	cell viability at 10^{-3} M (%)	EC_{50} (μM)	cell viability at 10^{-3} M (%)	EC_{50} (μM)	cell viability at 10^{-3} M (%)	EC_{50} (μM)
Ba(II)	NRK-52E	n. d.	n. d.	n. d.	n. d.	105.6 ± 5.1	>> 1000
	HEK-293	n. d.	n. d.	n. d.	n. d.	94.8 ± 3.4	>> 1000
Eu(III)	NRK-52E	89.6 ± 2.6	> 1000	74.1 ± 2.3	> 1000	59.8 ± 3.4	1050 ± 20
	HEK-293	97.5 ± 4.3	> 1000	78.1 ± 1.9	> 1000	57.9 ± 5.6	1020 ± 10
U(VI)	NRK-52E	54.0 ± 0.8	1070 ± 88	41.4 ± 2.1	757 ± 46	17.5 ± 0.9	533 ± 23
	HEK-293	72.1 ± 1.4	1920 ± 213	54.9 ± 4.4	1010 ± 59	29.0 ± 2.5	597 ± 38

n. d. = not determined.

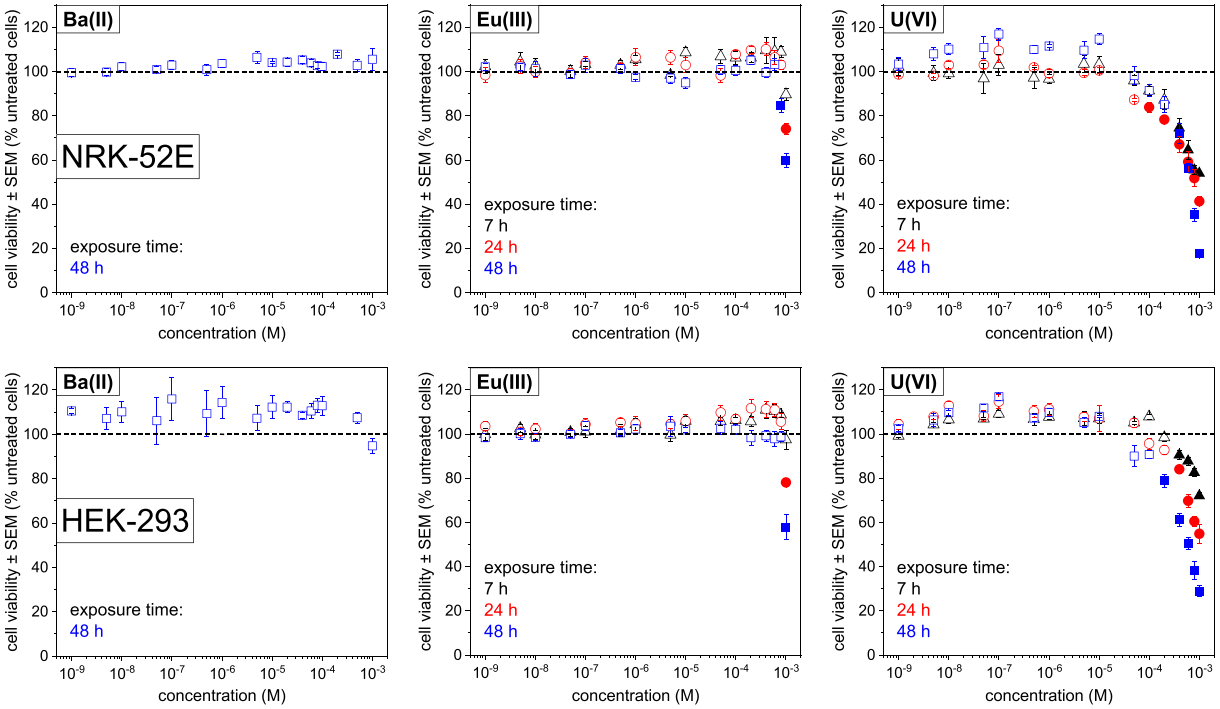

Fig. 1. Dose-response curves of Ba(II), Eu(III), and U(VI) after exposure of NRK-52E (upper row) and HEK-293 cells (lower row) for 7 h (black triangles, ▲), 24 h (red circles, ●), or 48 h (blue squares, ■). Filled symbols represent significances against untreated cells (calculated with $p < 0.05$). Untreated cells equal 100 % cell viability (dotted lines). Each value represents means ± SEM of three to five independent experiments.

response mechanisms. Another (more probable) one is a relation to the proliferation rate of the respective cell line: NRK-52E grow with a doubling time of approximately 13 h and therefore faster than HEK-293 (doubling time of approx. 21 h) (see ESI, Fig. S2). A higher proliferation rate probably leaves less time for repair of induced cell damage and, hence, results in higher susceptibility to cytotoxic effects. Different levels of intracellular metal accumulation could also be a conceivable cause. This is investigated in Section 3.3.

3.2. Morphological changes and cell death processes upon metal exposure

The morphological analyses and conducted bioassays focus only on NRK-52E since this cell line exhibits slightly higher sensitivity to metal exposure than HEK-293 (see Table 1). Untreated NRK-52E cells grow in a single monolayer, exhibit a cobblestone shape, and form close cell junctions (De Larco and Todaro, 1978). The single cell diameter is approximately 30–50 μm (see Fig. 2A). Exposure to 10^{-3} M Ba(II), Eu (III), and U(VI) leads to different changes in cell morphology, depending on the used heavy metal. Fluorescence microscopic images of untreated and heavy metal exposed NRK-52E cells are depicted in Fig. 2.

The major cell death pathways are apoptosis and necrosis. Apoptosis constitutes a regulated, programmed, and non-inflammatory process, while necrosis is characterized by spontaneous, unregulated, and inflammatory cell death. To distinguish between both processes, an annexin V apoptosis and necrosis differentiation assay was conducted. Additionally, caspase 3/7 activity (key enzyme for activation of regulated cell death processes) and cellular ROS generation (indicator for cellular stress and mitochondrial damage) were determined. The results of the bioassays are depicted in Fig. 3. The measured signals of metal exposed cells are always expressed as multiples of untreated control cells.

After exposure to 10^{-3} M Ba(II) for 48 h, the NRK-52E cells show an increase in cytoplasm volume and an enlarged diameter of up to 60 μm. The cell membranes appear dented in areas with high cell confluence, indicating cellular swelling (see red arrows in Fig. 2B). Nevertheless, overall cell morphology is unaltered and cell junctions are still intact. Hence, exposure to Ba(II) results in no detectable apoptotic or necrotic effect corresponding to the results of the viability experiments (see Table 1). Consistently, the results of the annexin V apoptosis and necrosis differentiation assay are below or equal to those of untreated cells (see Fig. 3A,B) and caspase 3/7 activity resembles that of normal control cells after 24 h (see Fig. 3C). However, ROS production is slightly increased to 1.4 ± 0.1 upon 24 h Ba(II) exposure (see Fig. 3D).

Regarding Ba(II) exposure, case studies on humans and experiments with rodents stated several structural changes in the kidneys, such as dilation of proximal tubules, intertubular hemorrhage, cloudy swelling of tubular epithelium, indentations of the renal capsule and deposition of amorphous granula (Ananda et al., 2013; Dietz et al., 1992; Mohammed and Ismail, 2017). The most striking cellular impact of Ba (II) is the competitive blockade of membrane potassium channels and the association with the Na^+-K^+-ATP pump, leading to high intracellular K^+ levels in tissues and concurrent hypokalemia in blood (Krishna et al., 2020; Roza and Berman, 1971; Schott and McArdle, 1974). Normally, potassium efflux is a cellular reaction to compensate hypoosmotic conditions across the plasma membrane but Ba(II) blocks this pathway and causes cellular swelling (Vogler et al., 2013). In experiments with Mueller cells from rats, 10^{-3} M Ba(II) was sufficient to trigger this effect (Vogler et al., 2013). Thus, a similar mechanism can be considered in our morphological studies. However, since the conducted XTT experiments do not reveal a significant loss in cell viability (see Table 1), the observed swelling does not seem to disturb fundamental cellular functions after 48 h exposure to Ba(II).

Although 10^{-3} M Ba(II) is not sufficient to induce apoptosis, necrosis, or significant viability decreases, the ROS assay indicates low level H_2O_2 production in kidney cells upon exposure for 24 h (see Fig. 3D). Changes in the antioxidant defense system of heart, blood, and lung cells upon $BaCl_2$ treatment are described in the literature. Decreased superoxide dismutase and catalase, reduced glutathione level, advanced oxidation protein product levels or increased lipid hydroperoxides are some of the main characteristics in this regard (Elwej et al., 2016, 2017; Omole

Table 2
EC_{50} values of various heavy metals after exposure of NRK-52E or HEK-293 for 24 h (sorted by increasing cytotoxicity). p. w. = present work.

Cell line	Element	Counterion	Exposure medium	EC_{50} (μM)	Reference
NRK-52E	Ba(II)	chloride	$DMEM^{P}$ + 10 % FBS	>> 1000[a]	p. w.
	Eu(III)	chloride	$DMEM^{P}$ + 10 % FBS	> 1000[b]	p. w.
	Eu(III)	chloride	DMEM + 10 % FBS	1080 ± 39	(Heller et al., 2019)
	Ni(II)	chloride	serum-free MEM	1050[c]	(Milgram et al., 2007)
	La(III)	chloride	DMEM + 10 % FBS	933 ± 25	(Heller et al., 2019)
	U(VI)	chloride	DMEM + 10 % FBS	902 ± 53	p. w.
	Yb(III)	chloride	DMEM + 10 % FBS	790 ± 28	(Heller et al., 2019)
	U(VI)	chloride	$DMEM^{P}$ + 10 % FBS	757 ± 46	p. w.
	U(VI)	bicarbonate	serum-free MEM	613[c]	(Milgram et al., 2007)
	U(VI)	nitrate	serum-free MEM	550[c]	(Thiébault et al., 2007)
	Co(II)	chloride	serum-free MEM	370[c]	(Milgram et al., 2007)
	U(VI)	citrate	serum-free MEM	350[c]	(Milgram et al., 2007)
	Ce(III)	chloride	DMEM + 10 % FBS	339 ± 29	(Heller et al., 2019)
	Cu(II)	chloride	serum-free MEM	260[c]	(Milgram et al., 2007)
	Zn(II)	chloride	serum-free MEM	55[c]	(Milgram et al., 2007)
	Cd(II)	chloride	$DMEM^{?}$ + 1 % FBS	3.9 ± 0.4	(Lee et al., 2017)
HEK-293	Ba(II)	chloride	$DMEM^{P}$ + 10 % FBS	>> 1000[a]	p. w.
	Eu(III)	chloride	DMEM + 10 % FBS	> 1470	(Heller et al., 2019)
	Eu(III)	chloride	$DMEM^{P}$ + 10 % FBS	> 1000[b]	p. w.
	Yb(III)	chloride	DMEM + 10 % FBS	1130 ± 76	(Heller et al., 2019)
	La(III)	chloride	DMEM + 10 % FBS	1070 ± 54	(Heller et al., 2019)
	Ce(III)	chloride	DMEM + 10 % FBS	1020 ± 66	(Heller et al., 2019)
	U(VI)	chloride	$DMEM^{P}$ + 10 % FBS	1010 ± 59	p. w.
	U(VI)	acetate	serum-free MEM	650[c]	(Carrière et al., 2004)
	U(VI)	bicarbonate	$DMEM^{?}$ + 1 % FBS	500[c]	(Prat et al., 2005)
	Cd(II)	chloride	$DMEM^{P}$ + 10 % FBS	44.8[d]	(Lawal and Ellis, 2010)

Exposure medium: no indicator = without pyruvate, ^{P} = with pyruvate;$^{?}$ = pyruvate unknown.
[a] Not able to calculate. Because of no effects even after 48 h, value estimated to be much higher than 1000 μM.
[b] Not able to calculate. Value must be higher than the highest applied concentration of 1000 μM.
[c] CI_{50} value (50 % loss of cell viability).
[d] IC_{50} value (50 % of the cells inhibited in growth).

et al., 2019). However, higher Ba(II) concentrations would be necessary to enhance this effect and cause severe disturbances in NRK-52E cells.

Exposure to 10^{-3} M Eu(III) for 48 h also leads to swelling and cytoplasm extension in NRK-52E cells. Cellular diameters range between 60 and 70 μm. Furthermore, the overall cell density is decreased and cell junctions are partially loose or lost. Additionally, plasma membrane fragmentation (see yellow arrows in Fig. 2C), the formation of blebs as well as the occurrence of apoptotic bodies (see red arrows in Fig. 2C) are visible. All these morphological changes are distinctive features of the apoptotic phenotype (regulated, non-inflammatory cell death) (Zhivotovsky, 2004). This corresponds very well to the caspase 3/7 results revealing a 3.0 ± 0.5 fold increase of protease activity upon Eu(III) exposure for 24 h (see Fig. 3C). Surprisingly, results of the annexin V apoptosis and necrosis assay are in contrast to that and mainly resemble those of Ba(II) exposed cells with values below or equal to the untreated control (see Fig. 3A,B). However, ROS generation is also elevated with 1.8 ± 0.3 fold changes compared to untreated cells at the same time point (see Fig. 3D).

In literature, several apoptotic effects of Ln on different cell types and a close relationship between generation of ROS and apoptosis induction are reported (Pałasz et al., 2019; Rim et al., 2013; Wang et al., 1999). According to this, Ln enter mitochondria *via* Ca^{2+} channels and cause alterations, *e.g.*, in pH, membrane potential, and ATP generation (Kajjumba et al., 2021). Mitochondrial impairments, in turn, provoke the generation of ROS and the release of cytochrome *c*, which activates caspases and finally leads to apoptosis induction (Liu et al., 2003, 2010; Wu et al., 2013). Our microscopic, caspase 3/7, and ROS results are in accordance with this. However, the absence of annexin V signals upon Eu(III) exposure is in contrast. A possible reason for this discrepancy is the chemical behavior of Eu^{3+} ions being known as Ca^{2+} analogs. The annexin V-phosphatidylserine interaction is Ca-dependent (Concha et al., 1992) and Ln^{3+} ions exhibit radii similar to Ca^{2+} (Reeves and Condrescu, 2003). Hence, Eu(III) may bind to the enzyme like Ca(II) and potentially impairs the affinity of annexin V to phosphatidylserine of apoptotic cells. This results in false low values and an underestimation of apoptosis. Therefore, for Eu(III), we consider the caspase 3/7 assay to be more reliable regarding the confirmation of apoptotic activity. The observed swelling of the cells after 48 h Eu(III) exposure is also uncharacteristic for apoptosis. One reason could be the mentioned Ln-Ca-analogy causing competitive replacements in binding proteins, regulatory defects of transport channels, and imbalances of Ca^{2+} levels (Liu et al., 2010; Reeves and Condrescu, 2003; Romero and Romero, 1999). Hence, ion homeostasis is probably disturbed and the presence of Eu(III) leads to osmotic impairments. Another reason could also be starting secondary necrosis, which arises in the absence of phagocytic activities in the *in vitro* cell culture and exhibits features of uncontrolled cell death, *e.g.*, cytoplasmic swelling (Vanden Berghe et al., 2010).

Exposure of NRK-52E cells to 10^{-3} M U(VI) leads to a high amount of swollen cells with increased diameters of up to 80–100 μm. Moreover, flattening of the plasma membrane (see red arrows Fig. 2D), loss of cell junctions, membrane deformation, rounding of cells, and reduced cell density are evident. In addition, the overall fluorescence intensity of the actin filament stain (Phalloidin) is decreased, indicating impairments of the cytoskeleton on a large scale. Compared to Ba(II) and Eu(III), U(VI) shows the strongest effects within the conducted bioassays. This corresponds to the viability assays, which indicate high cytotoxicity of U(VI) even at low concentrations (see Fig. 1). After 24 h, caspase 3/7 activity and ROS generation increase to 5.2 ± 0.4 and 3.0 ± 0.5 multiples of control cells, respectively (see Fig. 3C, D). Furthermore, the apoptosis and necrosis assay reveals time-dependent evolvement of both the annexin V and the DNA binding dye signals with opposite trends over time. The apoptosis signal is elevated in the first six hours of exposure, revealing 2.3 ± 0.4 (1 h) to 2.0 ± 0.1 (6 h) multiples of control cells. However, after 24 h, its intensity is strongly reduced and resembles that of untreated cells (see Fig. 3A). The necrosis signal, in turn, increases during the whole exposure time from 2.0 ± 0.1 multiples (1 h) to 5.0 ± 0.9 (48 h) (see Fig. 3B).

Extensive cellular swelling, membrane disruption, and cell rounding

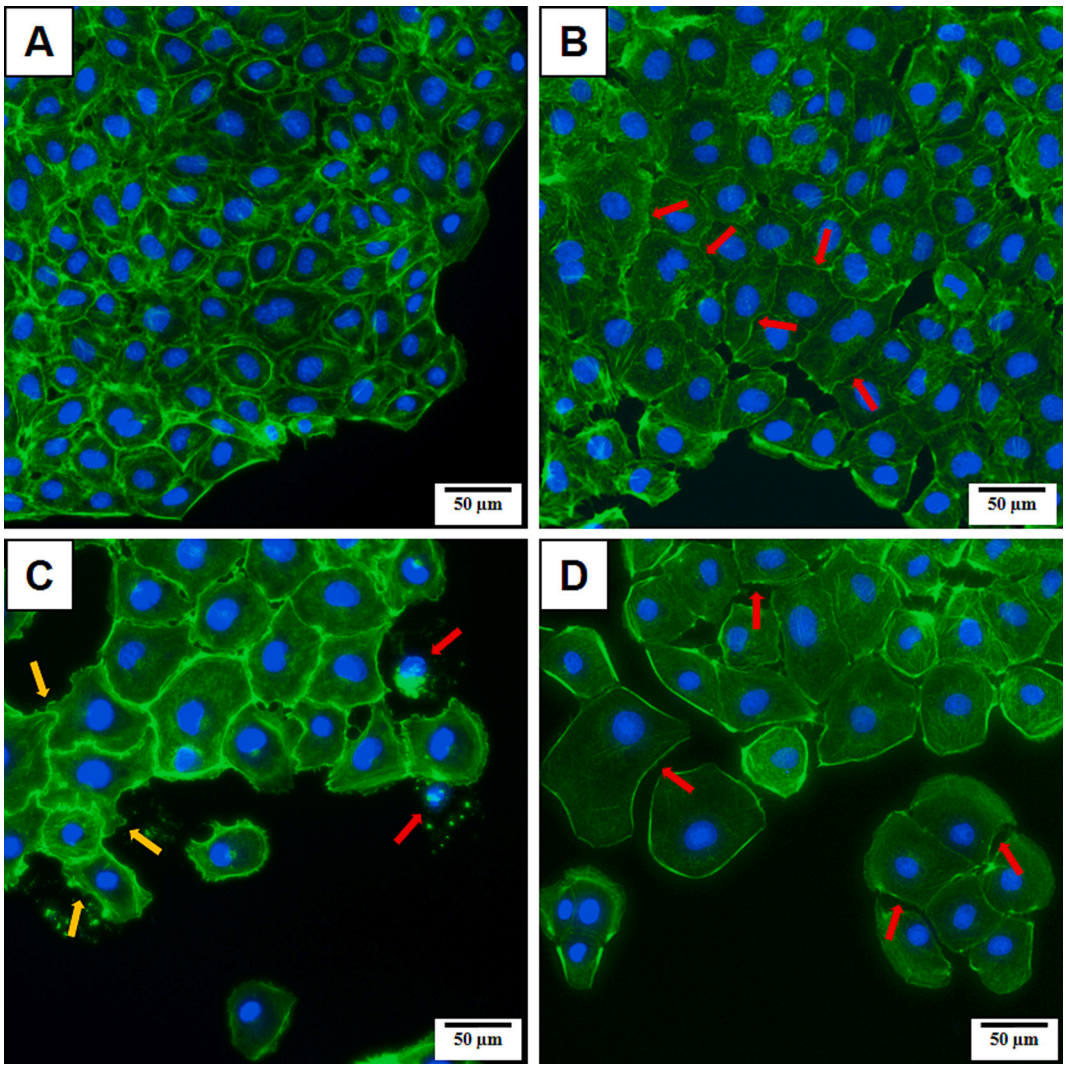

Fig. 2. Fluorescence microscopic images of NRK-52E cells after 48 h exposure: (A) untreated cells, (B) cells exposed to 10^{-3} M Ba(II), (C) 10^{-3} M Eu(III), and (D) 10^{-3} M U(VI). Images show overlays of DAPI (nucleus, blue) and Phalloidin-iFluor™ 488 Conjugate (cytoskeleton/actin, green) staining. Scale bars represent 50 µm. Arrows indicate swollen cells (B), plasma membrane fragmentation (C, yellow), apoptotic bodies (C, red) and flattening of the plasma membrane (D).

are morphological characteristics of necrosis, *i.e.*, spontaneous cell death with uncontrolled release of inflammatory contents (Vanden Berghe et al., 2010; Fink and Cookson, 2005). Consequently, the morphological analyses are in good agreement with the annexin V apoptosis and necrosis assay indicating dominant necrotic cell death after ≥ 24 h of treatment. Likewise, a study of Thiébault et al. (2007) in serum-free MEM also suggests necrosis of NRK-52E cells after 24 h exposure to elevated U(VI) concentrations, being accompanied by low caspase 3 activity and intense ROS generation. The latter is in line with our bioassay results indicating elevated ROS levels compared to untreated control cells, probably arising due to mitochondrial damage (Thiébault et al., 2007; Yuan et al., 2016).

However, in contrast to the annexin V and necrosis assay, our results also yield highly increased caspase 3/7 activity after 24 h, constituting a key feature of regulated processes. This does not match necrotic cell death and indicates the contribution of other molecular pathways at this point. In this regard, a study by Zheng et al. (2022) suggests pyroptosis induction in NRK-52E cells upon treatment with $5{\cdot}10^{-4}$ M U(VI) for 24 h. This more recently described regulated form of inflammatory cell death is characterized by pore formation in the plasma membrane, which leads to water influx, cell swelling, and osmotic membrane disruptions (Vande Walle and Lamkanfi, 2016; Wang et al., 2022; Yu et al., 2021). Flattening of the plasma membrane caused by membrane leakage is also described (Yu et al., 2021). Although necrosis and pyroptosis differ greatly in their activation and molecular characteristics, morphological differentiation of these processes has certain limitations.

Pyroptosis is mediated by caspase-induced cleavage of the protein gasdermin, which induces pore formations in the cell membrane (Kovacs and Miao, 2017). Interestingly, also caspase 3 is capable to activate gasdermin cleavage and, thus, induce pyroptosis (Kovacs and Miao, 2017; Wang et al., 2017). Due to the early membrane rupture upon pyroptosis, phosphatidylserine is exposed in the inner leaflet and can bind to annexin V (Vande Walle and Lamkanfi, 2016). This leads to annexin V staining of apoptotic as well as pyroptotic cells. Furthermore, these cells can also be stained by necrosis detection dyes, which enter the cells due to the disturbed membrane integrity and bind to the DNA (Vande Walle and Lamkanfi, 2016). Hence, pyroptotic cells are annexin V^+/DNA dye^+ stained, while apoptotic cells exhibit annexin V^+/DNA dye^- staining and necrotic cells are annexin V^-/DNA dye^+ stained (Vande Walle and Lamkanfi, 2016; Wang et al., 2017). However, the signal combination upon U(VI) exposure in our study (annexin V^-/DNA dye^+ cell signals with high caspase 3/7 activity after 24 h) suggests simultaneous or overlapping occurrence of pyroptotic and necrotic cell death after 24 h and further investigations are needed for a more detailed characterization.

In summary, 10^{-3} M Ba(II), Eu(III), and U(VI) cause different

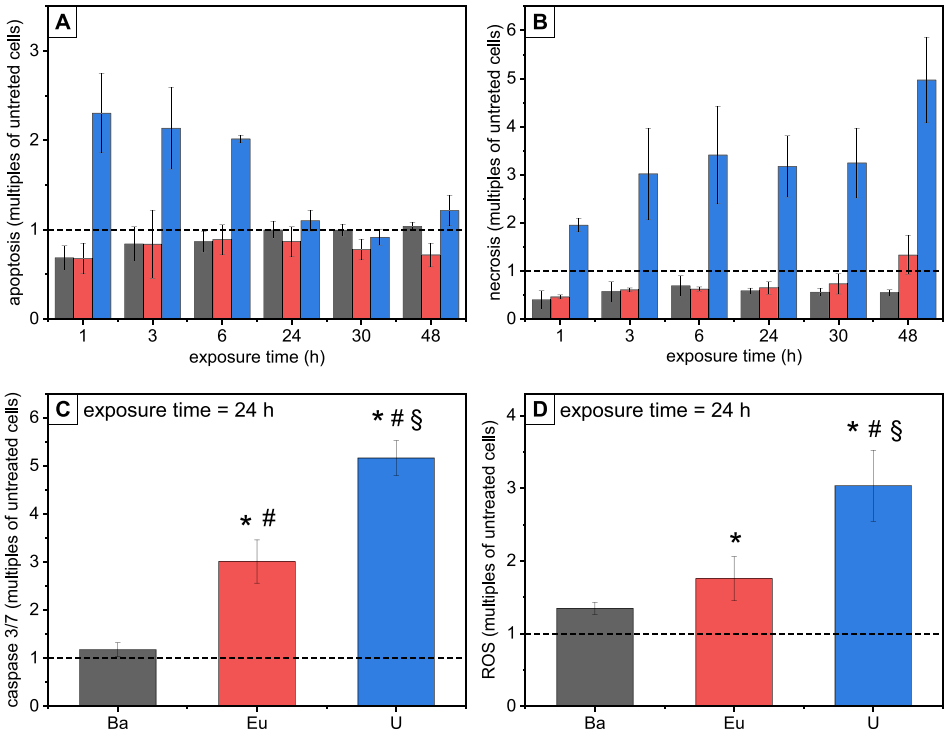

Fig. 3. Signals of annexin V (A) and DNA binding dye (B), caspase 3/7 activity (C) and ROS production (D) in NRK-52E cells upon exposure to 10^{-3} M Ba(II) (grey), Eu(III) (red), or U(VI) (blue). All values are expressed as multiples of untreated control cells (dotted lines). Each bar represents means ± standard derivation of at least three independent experiments. * = significance against untreated cells; # = significance against Ba(II); § = significance against Eu(III). All significances were calculated with $p < 0.05$.

morphological effects as well as ROS generation and caspase 3 activation in kidney cells. The intensity of the impact ranks Ba(II) < Eu(III) < U (VI). While Ba(II) causes only disturbance of the osmotic equilibrium, Eu (III) and U(VI) exposure leads to severe damage and cell death induction *via* apoptotic or necrotic/pyroptotic pathways, respectively.

3.3. Intracellular metal uptake

The intracellular uptake of Ba(II), Eu(III), and U(VI) into NRK-52E and HEK-293 cells, respectively, was determined by ICP-MS after cell lysis using each two different metal concentrations (10^{-5} and 10^{-3} M). Results of 10^{-3} M are given in Fig. 4, those of 10^{-5} M in the ESI, Fig. S3. All data are summarized in the ESI, Table S3.

As can be seen in Fig. 4, the intracellular amount of Ba(II), Eu(III), and U(VI) differs significantly depending on the metal ion. For both cell lines as well as for all exposure times, Ba(II) is by far the least accumulated element into the cells. In addition, the amount of intracellular Ba(II) remains almost constant throughout the exposure period at 12 ± 4 ng Ba(II)/10^6 cells for NRK-52E and 38 ± 4 ng Ba(II)/10^6 cells for HEK-293. Thus, Ba(II) uptake into NRK-52E and HEK-293 cells is independent from time. Eu(III) and U(VI), on the other hand, both exhibit a time-dependent accumulation with increasing intracellular amount at prolonged exposure time. In NRK-52E cells, the amount of Eu(III) increases from 49 ± 8 at 6 h to 237 ± 8 ng/10^6 cells after 48 h, whereas in the HEK-293 cells a maximum of 200 ± 11 ng/10^6 cells is apparently reached after 24 h. Eu(III) uptake does not further increase significantly

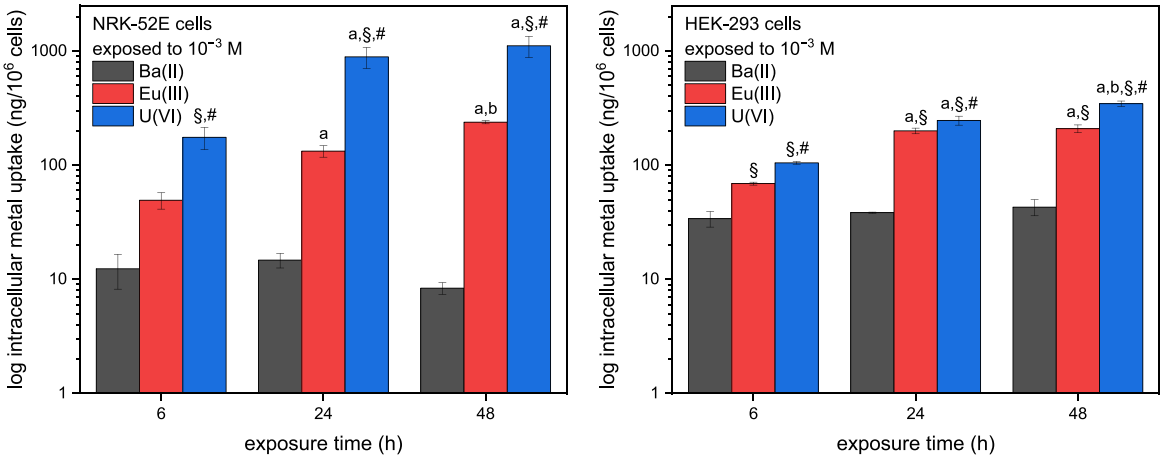

Fig. 4. Intracellular metal uptake of 10^{-3} M Ba(II), Eu(III), and U(VI) into NRK-52E (left) and HEK-293 cells (right) after different exposure times. Data represent mean values of three independent experiments ± SD with all samples in duplicate. § = significant against Ba, # = significant against Eu, a = significant against 6 h, b = significant against 24 h. All significances were calculated with $p < 0.05$.

upon exposure for 48 h. In contrast, the intracellular uptake of U(VI) increases from 176 ± 39 (NRK-52E) and 105 ± 3 ng/10^6 cells (HEK-293) after 6 h exposure to 1113 ± 234 (NRK-52E) and 346 ± 19 ng/10^6 cells (HEK-293) after 48 h, respectively.

Remarkably, NRK-52E cells accumulate significantly higher amounts of U(VI) than HEK-293 cells. Since it is known that in some bacterial species, such as *Thiobacillus ferrooxidans*, only a small amount of U(VI) can be extracted from the biomass using EDTA (Panak et al., 1999), experiments were repeated for both cell lines with HEDP as washing agent to exclude an incomplete removal of the membrane-bound U(VI) during trypsinization of the NRK-52E cells. HEDP is a proposed decorporation agent, as it exhibits a very high affinity to U(VI) and shows promising results in *in vitro* and *in vivo* animal experiments after U(VI)-contamination (Henge-Napoli et al., 1999; Jacopin et al., 2003; Martínez et al., 2000; Tymen et al., 2000). However, the results of cells washed with HEDP are comparable to those of cells washed with trypsin/EDTA (see ESI, Fig. S4). Therefore, it can be concluded that incomplete removal of U(VI) sorbed to the cell membrane through trypsinization is unlikely to have occurred. Thus, the intracellular U(VI) uptake results indicate that the higher U(VI) cytotoxic susceptibility of NRK-52E cells compared to HEK-293 (see Table 1), most probably is due to the higher U(VI) uptake into NRK-52E cells.

In addition to the exposure time, the metal concentration also influences the intracellular uptake of Eu(III) and U(VI). In cells exposed to 10^{-5} M, *e.g.*, 1 ± 0.2 ng Eu(III)/10^6 cells or 2.0 ± 0.1 ng U(VI)/10^6 cells are taken up by HEK-293 cells after 24 h (see ESI, Fig. S1). The differences in the intracellular amounts between the metals most probably arises from different mechanisms of intracellular uptake due to the different oxidation states. Ba(II) blocks potassium channels and associates with the Na^+-K^+-ATP pump (Krishna et al., 2020). Hence, the uptake of Ba(II) *via* ion channels is probably only very small and limited, which can be the reason for the low but constant accumulation in the cells. In the case of Ln, the following mechanisms are discussed to be involved in intracellular uptake in mammalian cells: uptake by i) Na^+-Ca^{2+}-exchanger due to the very similar physicochemical properties of Ln^{3+} and Ca^{2+} ions (Pallares et al., 2020; Reeves and Condrescu, 2003), ii) ionophores (Wang et al., 1998), iii) permeabilisation of the plasma membrane (Cheng et al., 1999), and iv) endocytosis (Du et al., 2002). One or more of these mechanisms are, therefore, likely to be responsible for the intracellular uptake of Eu(III) into renal cells. Last but not least, for U(VI), both membrane transporters and endocytosis are assumed to be involved in intracellular accumulation in renal cells, with soluble U(VI)-carbonate or phosphate complexes being taken up by membrane transporters and/or endocytosis, whereas precipitated U(VI)-phosphate is probably incorporated only by endocytosis (Carrière et al., 2008). The study by Huang et al. (2023) suggests that endocytotic U(VI) uptake in HK-2 cells is mainly mediated by clathrin, although the caveolae-dependent endocytosis pathway may also be involved. Both mechanisms have also been shown to be involved in U(VI) uptake in other cells, *e.g.*, sodium-dependent phosphate co-transporters and endocytosis are involved in the intracellular uptake of U(VI) in LLC-PK_1 cells (Muller et al., 2006, 2008). Finally, the heavy metals' speciation also influences intracellular uptake (Sachs et al., 2015) and is, therefore, investigated in more detail in Section 3.4.

In summary, the results of intracellular metal uptake correlate very well with the results of the cell viability experiments (see Table 1). This indicates that the cytotoxic effects strongly depend on the amount of metal accumulated. The same trend has been observed in other cell lines, *e.g.*, in HK-2 and FaDu cells (Huang et al., 2023; Sachs et al., 2015). However, in FaDu cells after exposure to 10^{-3} M Eu(III) for 24 h, with 0.03 ng/10^6 cells (Sachs et al., 2015), the Eu(III) uptake is significantly lower than in NRK-52E cells (132 ± 15 ng/10^6 cells). In contrast, U(VI) uptake in HK-2 cells from the study of Bao et al. (2013) agrees very well with the results of HEK-293 cells in this study. After 24 h exposure of cells to 10^{-3} M U(VI), about 6.5 ng/10^6 cells were taken up in HK-2 cells (Bao et al., 2013) (compared to 2.0 ± 0.1 ng U(VI)/10^6 cells in HEK-293 in our study). An altered mode of action due to the use of acetate as a counterion to U(VI) for HK-2 cells could explain the small differences (see Table 2). However, for NRK-52E cells, there is a large discrepancy between the U(VI) uptake in our study (1.4 ng/10^6 cells, 10^{-5} M U(VI)) and the literature, which ranges from 100 to 350 ng U(VI)/10^6 cells after 48 h of exposure to 1.2•10^{-5} M U(VI) (Chen et al., 2022; Shi et al., 2022; Wang et al., 2019, 2020). Since, on the one hand, our data of HEK-293 cells agree well with the results of NRK-52E cells as well as with the literature for HK-2 cells and, on the other hand, the cited data are from one and the same research group (presumably from one experiment), we assume that the clear differences are due to a different procedure in cell preparation/washing and the data are, therefore, not directly comparable with our results.

3.4. Solubility and thermodynamic modelling of barium(II), europium (III), and uranium(VI) speciation in cell culture medium

Since the solubility of the metals has an important influence on bioavailability and, thus, on the effect of the metals on the cells, the solubility of Ba(II), Eu(III), and U(VI) in the cell culture medium was investigated. Therefore, metal solutions ($5{\cdot}10^{-4}$–10^{-3} M) were prepared in cell-free medium and incubated under the same conditions like in cell culture experiments for 24 and 48 h, respectively. After filtration through 0.2 μm sterile filters (Eu(III) and U(VI)) or ultracentrifugation (Ba(II)), the concentrations were measured by ICP-MS. The results are shown in Fig. 5.

The solubility of Ba(II), Eu(III), and U(VI) in the cell culture medium is very high over the entire concentration range investigated and no visible precipitates were detected. In addition, solubility is independent from incubation time. This indicates that the metal ions form soluble complexes in the cell culture medium and are, therefore, bioaccessible for the cell.

Complexation of Ba(II) is known for several components of the cell culture medium. In the case of inorganic components, Ba(II) forms complexes, *e.g.*, with carbonate (logK = 2.71 for $BaCO_3$(aq)) (Busenberg and Plummer, 1986) and sulfate (logK = 2.7 for $BaSO_4$(aq)) (Felmy et al., 1990). The available data for complexation of Ba(II) with organic compounds of the cell culture media are sparse. For the amino acids present in cell culture media, a complex of Ba(II) with glycine (logK = 0.4) has been reported in the past (Smith and Martell, 1987). Beside these soluble complexes, Ba(II) is well known for the formation of insoluble salts. Precipitation of Ba(II) salts, such as $BaSO_4$(s) ($\log K_{sp}$ = −9.97) (Blount, 1977) or $BaCO_3$(s) ($\log K_{sp}$ = −8.56) (Busenberg and Plummer, 1986), was therefore to be expected. The results of the thermodynamic modeling are shown in the ESI, Fig. S5. PhreeqC predicts, depending on pH, > 80 % of Ba(II) to be precipitated due to the low solubility limit of $BaSO_4$.

The surprisingly high solubility of Ba(II) in the cell culture medium determined in our experiments cannot be fully explained at this point. The proteins of the FBS can be excluded as the source of the high solubility of Ba(II), since no precipitates were observed in serum-free DMEM with 10^{-3} M Ba(II), too. Furthermore, no precipitates were detected in experiments with a mixture of only the inorganic medium components (see ESI, Table S1), suggesting that one or more inorganic salts must be responsible for the solubility of Ba(II) in the cell culture medium. Hence, continuative precipitation experiments with different inorganic salts mixtures were performed (see ESI, Table S4). So far, it seems that a combination of carbonate, phosphate, and presumably chloride might be responsible for the Ba(II) high solubility. However, further investigations are required to clarify this issue.

The thermodynamic modeling of Eu(III) and U(VI) in cell culture medium has already been discussed in detail in the literature (Heller et al., 2019; Milgram et al., 2008). Briefly, at 10^{-3} M, Eu(III) is predicted to precipitate as phosphate and (hydroxy)carbonate minerals, whereas, when precipitation is suppressed, speciation is dominated mainly by carbonate, phosphate, and hydrogen phosphate species (Heller et al.,

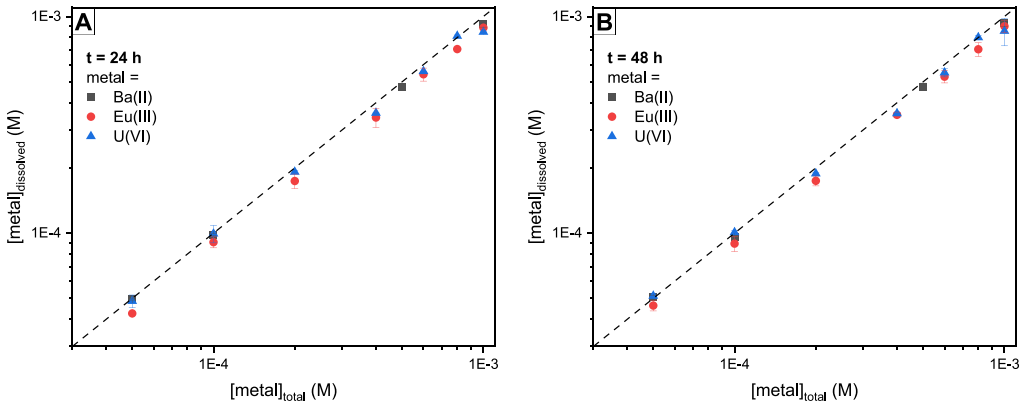

Fig. 5. Solubility of Ba(II), Eu(III), and U(VI) in the cell culture medium after incubation for 24 (A) and 48 h (B). The dashed line is the theoretical line of 100 % solubility. Data represent mean values of two experiments ± SD.

2019). Nevertheless, it has also been demonstrated, that experimental solubility is much higher than the thermodynamically modeled one due to a lack of data for Eu(III) complexes with organic medium components and proteins (Heller et al., 2019). At 10^{-3} M U(VI), the speciation is predicted to be dominated by carbonate species, mainly $UO_2(CO_3)_3^{4-}$ and $UO_2Ca_2(CO_3)_3$(aq) (Milgram et al., 2008).

In summary, our solubility results of Eu(III) and U(VI) agree well with experimental literature data while the unexpected high solubility of Ba(II) needs further elucidation.

3.5. Speciation of barium(II), europium(III), and uranium(VI)

The speciation of a metal strongly determines its solubility and bioavailability and, thus, influences its effect on cells as well as its intracellular uptake. It is, therefore, crucial to know the solubility and speciation of metal ions in order to better understand biological and biochemical processes. Speciation studies of Ba(II) were conducted using ESI-MS. As this method does not allow the measurement of cell suspensions, Ba(II) speciation was only investigated in the cell culture medium.

Solutions of the cell culture medium containing 10^{-5} or 10^{-3} M Ba (II) were measured with ESI-MS immediately after sample preparation and after 48 h (see Fig. 6).

No significant complexation of Ba(II) with components from the cell culture medium could be detected after 48 h (see ESI for media composition, Table S1), whereas the dominant species was found to be the non-complexed Ba^{2+} ion (see Fig. 6). Adducts from the ESI-process of Ba(II) with water and carbohydrates, such as glucose, could be found in the mass spectra and were assigned to the Ba^{2+} ion. In agreement with the thermodynamic modeling (see Fig. S5 in the ESI), Ba^{2+} appears to be the dominant soluble species. Other species, such as $BaHCO_3^+$ could not be identified in solution by ESI-MS. This could be due to their abundance being below the detection limit or the signal-to-noise ratio being too low, so that a clear identification is not possible. Another possibility would be the formation of neutral complexes, which cannot be detected with ESI-MS. Exchange of CO_2 with an 5 % CO_2 atmosphere was included in the thermodynamic modelling. Given the contact of the cell culture medium with regular atmosphere for ESI-MS measurements, a deviating abundance of $Ba(CO_3)$ and $Ba(HCO_3)^+$ in solution could therefore explain this observation.

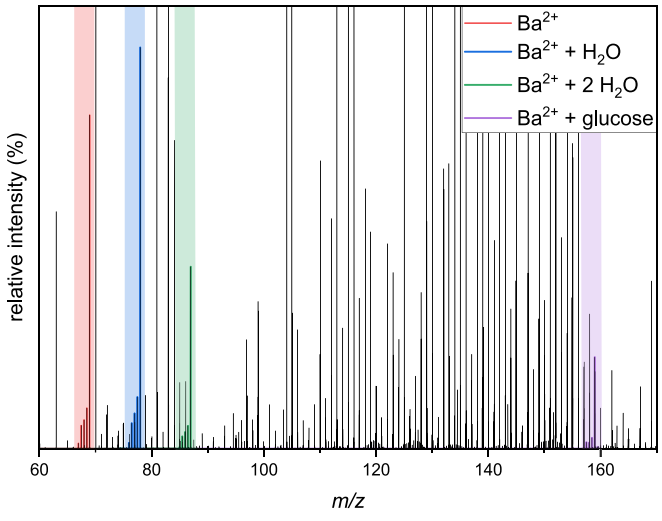

Fig. 6. Positive ion ESI-MS spectrum of 10^{-3} M Ba(II) in cell culture medium after 48 h. Peak groups associated with Ba^{2+} and its adduct species formed during the ESI-process are shown in color.

TRLFS was used to study Eu(III) and U(VI) speciation as it is an excellent method for both elements due to their outstanding luminescence properties. Emission spectra were recorded for both metal ions (10^{-5} and 10^{-3} M) in pyruvate containing cell culture medium, medium supernatants of metal exposed cells (subsequently only called supernatants) as well as in suspensions of Eu(III) or U(VI) exposed cells.

The steady-state spectra of 10^{-3} and 10^{-5} M Eu(III) in cell culture medium, medium supernatants of exposed cells, and cell suspensions after exposure for 24 h are shown in Fig. 7. Data for 48 h exposure are given in the ESI, Fig. S6. Since the results of the supernatants of Eu(III) exposed NRK-52E cells are nearly identical to those of the supernatants of exposed HEK-293 cells, only the former data are shown. All spectral parameters are compiled in the ESI, Table S5.

Compared to the Eu^{3+} aqua ion, a small $^7F_0$ peak appears in the spectra at both Eu(III) concentrations in cell culture medium and supernatants of exposed cells. This indicates a slight distortion in the symmetry of the metal center. Furthermore, there is a strong enhancement of the $^7F_2$ peak provoking an increase in the $R_{E/M}$ as well as a splitting of the $^7F_4$ band. Overall, at constant Eu(III) concentration, there are no significant differences between the spectra of Eu(III) in the cell culture medium and in the supernatants of the exposed cells.

At 10^{-3} M Eu(III) (Fig. 7A), PARAFAC evaluation of the measured TRLF spectra revealed that one and the same species is formed in pyruvate containing cell culture medium and supernatants of exposed cells. This Eu(III) species 1 (red) is characterized by a $R_{E/M}$ of 1.7 ± 0.1, a strong splitting of the $^7F_4$ band, and a luminescence lifetime of 543 ± 4 μs (Fig. 8A,B) corresponding to 1.5 ± 0.5 water molecules left in the metal's first coordination sphere.

In suspensions of cells exposed to 10^{-3} M Eu(III), TRLF spectra similar to those in cell-free medium were recorded (Fig. 7A). Interestingly, there are no significant differences in the Eu(III) luminescence

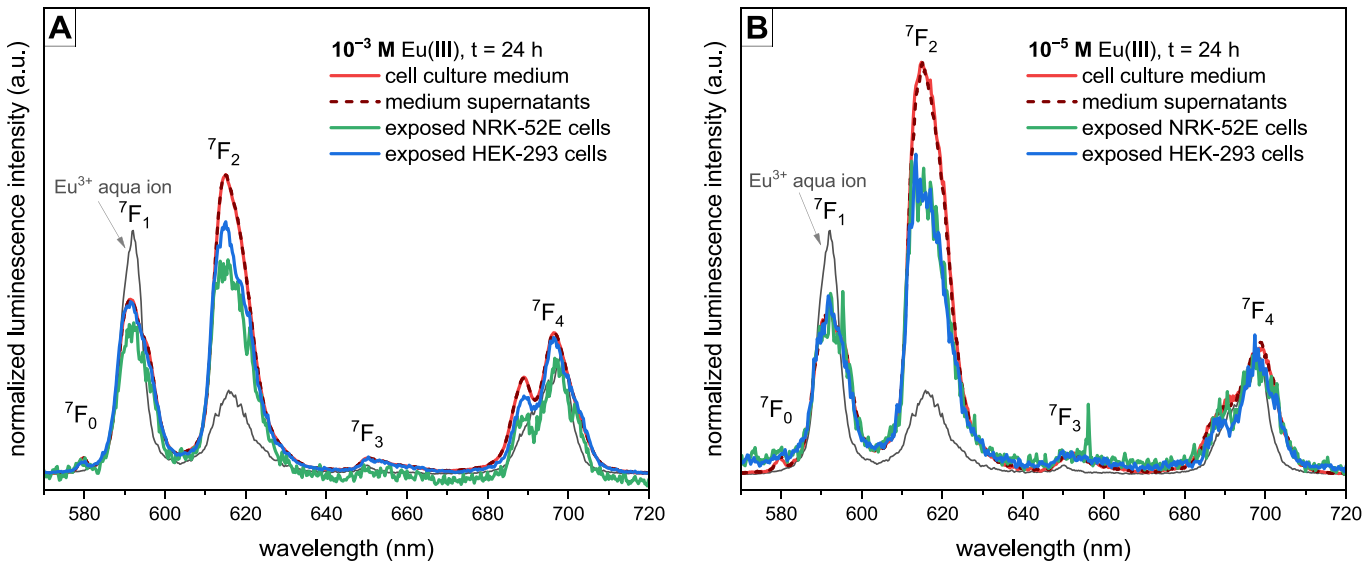

Fig. 7. Steady-state luminescence spectra of 10^{-3} (A) and 10^{-5} M Eu(III) (B) in cell culture medium, in medium supernatants of exposed cells, and in cell suspensions after exposure for 24 h. All steady-state spectra were normalized to the same area of the $^7F_1$ band.

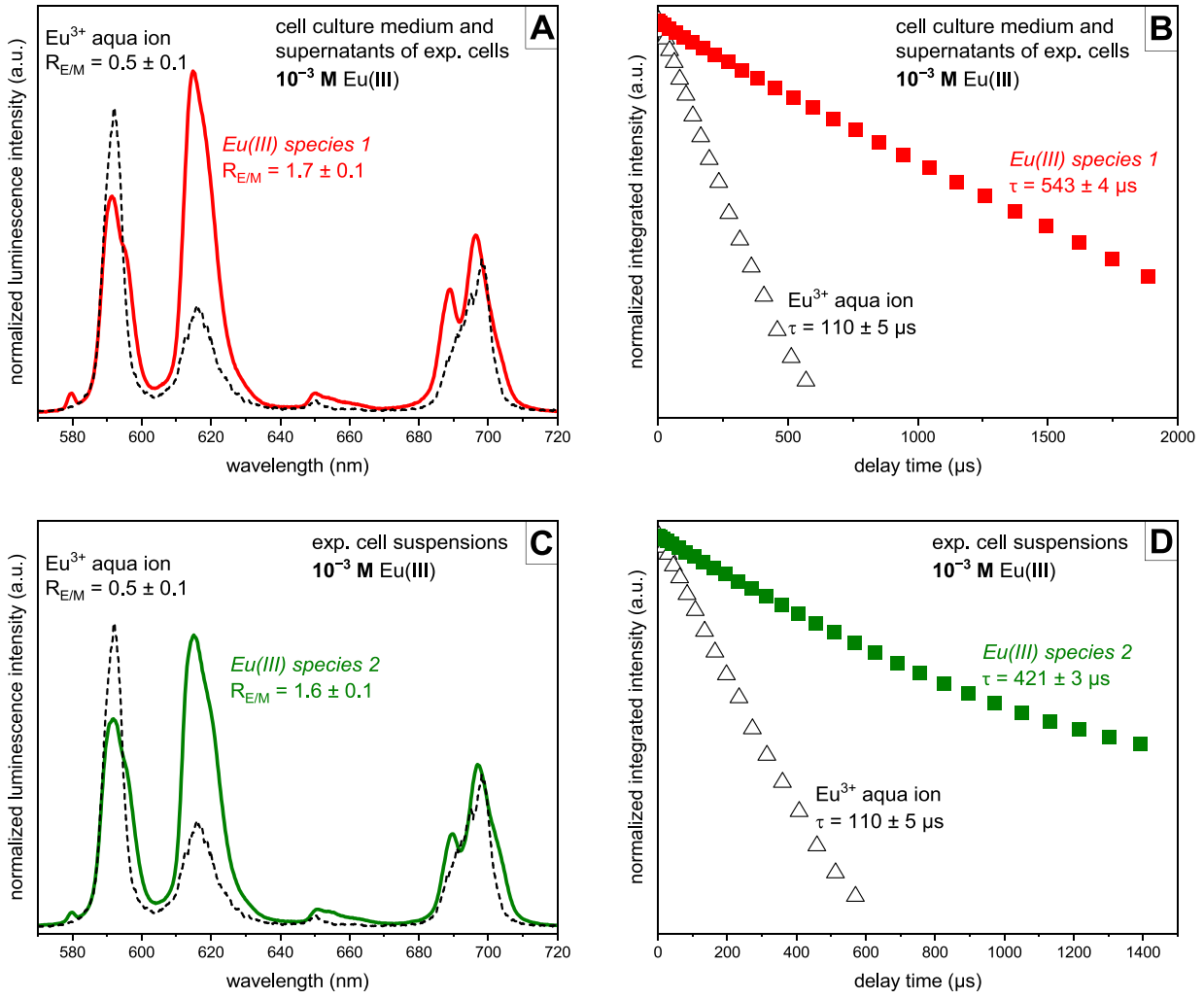

Fig. 8. PARAFAC results of TRLFS series of 10^{-3} M Eu(III) in cell culture medium and supernatants of exposed NRK-52E cells (A, B) as well as in exposed cell suspensions (C, D). Emission spectra (A,C) and luminescence decay curves (B,D).

spectra between both cell lines. Only the signal-to-noise ratio of the spectra recorded in exposed NRK-52E cell suspensions is lower compared to those measured in exposed HEK-293 cell suspensions. This is due to a lower cell density of the NRK-52E cells and, hence, a lower Eu (III) concentration in exposed cell suspensions. PARAFAC evaluation revealed a Eu(III) species 2 (green) characterized by a $R_{E/M}$ of 1.6 ± 0.1 and τ = 421 ± 3 μs (Fig. 8C,D) corresponding to 2.1 ± 0.5 water molecules left in the first hydration shell of the metal ion.

At 10^{-5} M Eu(III), some differences occur in the TRLF spectra, *i.e.*, a higher $R_{E/M}$ and a less pronounced splitting of the $^7F_4$ peak (Fig. 7B). Furthermore, data evaluation was not that straight forward and more complex. PARAFAC results indicate the simultaneous formation of two different Eu(III) species in both cell culture medium and supernatants of exposed cells (Fig. 9). Eu(III) species 3 (blue) exhibits a high $R_{E/M}$ of 3.4 ± 0.1 and τ = 387 ± 8 μs corresponding to 2.3 ± 0.5 water molecules (Fig. 9A,B). In contrast, Eu(III) species 4 (orange) has a lower $R_{E/M}$ of 2.1 ± 0.1 and a longer luminescence lifetime of 578 ± 11 μs equaling 1.4 ± 0.5 water molecules remaining in the first coordination shell of the metal ion (Fig. 9A,B).

In suspensions of cells exposed to 10^{-5} M Eu(III), TRLF spectra similar to those in cell-free medium were recorded (Fig. 7B). Interestingly, there are, again, no differences in the Eu(III) luminescence spectra between both cell lines. PARAFAC evaluation revealed two co-existing Eu(III) species. These are Eu(III) species 2 (green) which is also found in cell-free medium at higher Eu(III) concentration as well as a new Eu (III) species 5 (magenta) which is characterized by a $R_{E/M}$ of 3.0 ± 0.1 and a luminescence lifetime of 237 ± 16 μs corresponding to 4.0 ± 0.5 water molecules remaining in the first hydration shell of the metal ion (Fig. 9C,D).

Assignment of the described Eu(III) species and potential binding motifs was achieved by comparison of our results with experimental and literature data of, on the one hand, Eu(III) with organic and inorganic model ligands and, on the other hand, Eu(III) in plant and bacterial cells (Günther et al., 2022; Hilpmann et al., 2023; Jessat et al., 2023; Klotzsche et al., 2023; Stadler et al., 2023; Vogel et al., 2021). Representative TRLF spectra of Eu(III) complexes with model ligands representing carboxylate, organophosphate, and inorganic phosphate binding are given in the ESI, Fig. S7.

Luminescence spectra of Eu(III) species 1 (red) and 2 (green) are very similar in the overall shape and exhibit nearly identical $R_{E/M}$ as well as water molecules left in the first coordination sphere of the Eu^{3+} ion (see Fig. 8). We, therefore, assume that the same type of ligand/binding motif is present in both Eu(III) species. Due to the significant splitting of the $^7F_4$ band, we assign these two species to an inorganic phosphate complexation of Eu(III). TRLF spectra of $EuPO_4$ reveal the same characteristic splitting of the $^7F_4$ band (see ESI, Fig. S7C) (Stadler et al., 2023). The slightly higher lifetimes as well as the higher $R_{E/M}$ of Eu(III) species 1 (red) and 2 (green) compared to $EuPO_4$ can be explained by i) the complex composition of both the cell culture medium and the cellular matrix, ii) the formation of a Eu(III) polyphosphate species, or

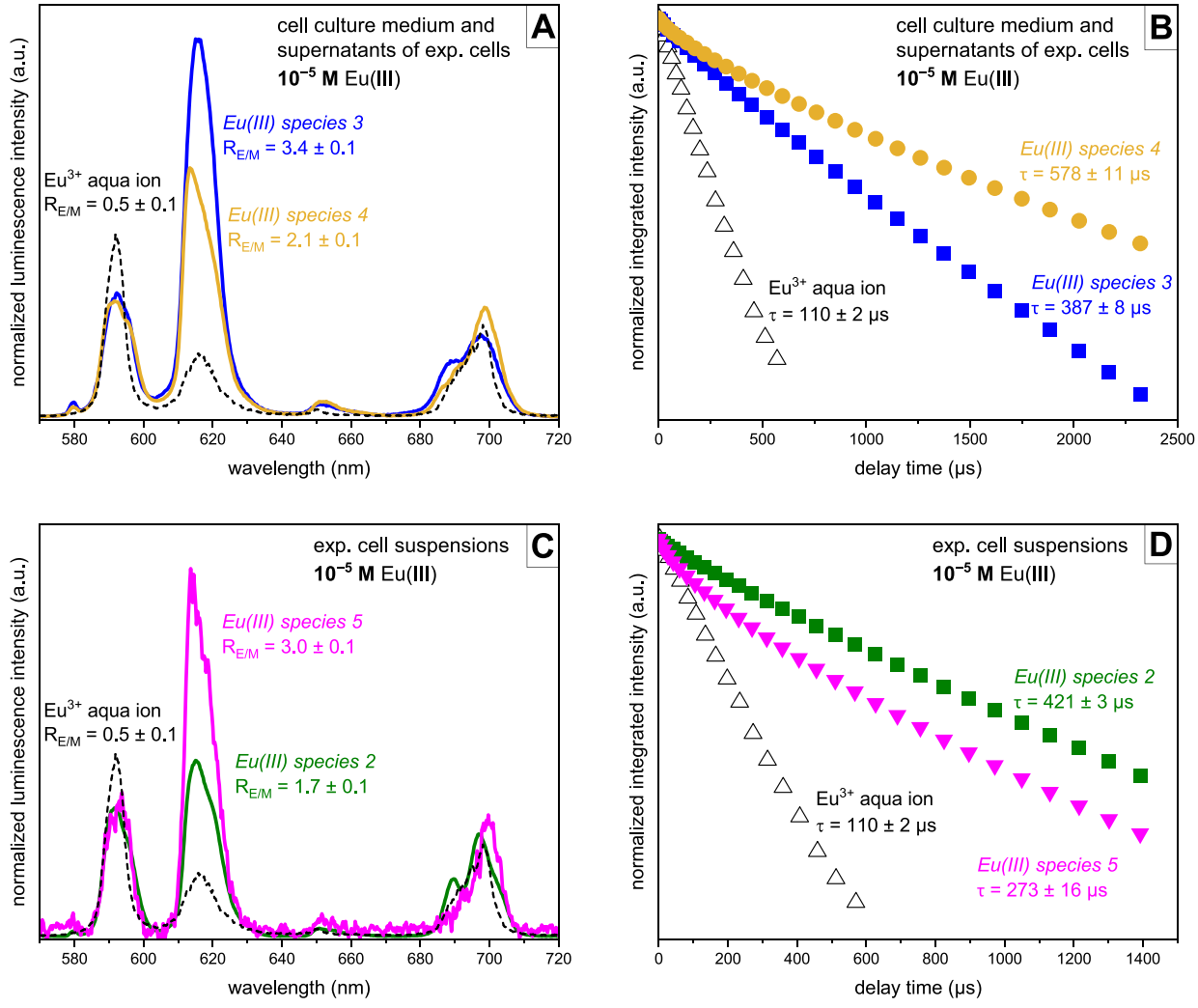

Fig. 9. PARAFAC results of TRLFS series of 10^{-5} M Eu(III) in cell culture medium and supernatants of exposed NRK-52E cells (A, B) as well as in cell suspensions (C, D). Emission spectra (A, C) and luminescence decay curves (B, D).

iii) by the binding of an additional (in-) organic ligand in the Eu(III) phosphate complex. Such mixed or ternary Eu(III) complexes, *e.g.*, with both phosphate and carbonate, are already reported to form in natural saliva (Barkleit et al., 2017) as well as natural human urine at pH > 5.8 (Heller et al., 2011). The TRLF spectra of the ternary Eu(III) complexes in those two biological media exhibit similar $R_{E/M}$ and luminescence lifetimes like Eu(III) species 1 (red) and 2 (green). Furthermore, phosphate is not only a ubiquitous and important component of DNA/RNA and cellular proteins but also the main inorganic component of the cell culture medium supplement FBS (Lee et al., 2022). This strongly supports our assignment. Finally, the TRLF spectra of Eu(III) species 1 (red) and 2 (green) are in very good agreement with those of Eu(III) in winter rye (magenta species in *Secale cereale* L. (Stadler et al., 2023)), in various fungi (magenta species in *Schizophyllum commune*, *Pleurotus ostreatus*, *Lentinus tigrinus* as well as *Leucoagaricus naucinus* (Günther et al., 2022)), and in a sulfate-reducing bacterium (magenta + red species in *Desulfosporosinus hippei* DSM 8344^T (Hilpmann et al., 2023)), which were all assigned to inorganic phosphate binding of Eu(III) inside the cells.

The TRLF spectrum of Eu(III) species 3 (blue) is mainly characterized by its high $R_{E/M}$ (see Fig. 9). All spectroscopic parameters are nearly identical to those of a proteinaceous Eu(III) species reported on the surface of the metal-reducing bacterium *Shewanella oneidensis* (Vogel et al., 2021). Furthermore, Eu(III) complexation with the intracellular receptor protein calmodulin yields TRLF spectra with similar $R_{E/M}$ and luminescence lifetime (binding sites 2–4 (Drobot et al., 2019)). Finally, also TRLF spectra of Eu(III) in roots of winter rye (yellow species in *Secale cereale* L. (Stadler et al., 2023)), in roots of rapeseed (blue species in *Brassica napus* (Jessat et al., 2023)), and in aqueous solution of 10 % FBS + carbonate (Heller et al., 2019), which were all assigned to protein binding of Eu(III), exhibit comparable luminescence parameters. Hence, Eu(III) species 3 (blue) is assigned to be an Eu(III)-protein complex.

In the case of Eu(III) species 4 (orange) and 5 (magenta), the measured TRLF spectra exhibit similarities in the overall shape (see Fig. 9). Therefore, we assume that the same type of ligand/binding motif is present in both Eu(III) species. With regard to the shape of the sensitive $^7F_2$ and $^7F_4$ bands, we assign these two species to an organic phosphate complexation of Eu(III). Comparison with TRLF spectra of Eu(III) complexes with the organophosphate model ligands phosvitin, phytate, and RNA (Vogel et al., 2021) reveals very similar shape of both the $^7F_2$ and $^7F_4$ bands as well as a comparable $R_{E/M}$ (see ESI, Fig. S7B). Again, slight differences in the spectroscopic parameters of Eu(III) species 4 (orange) and 5 (magenta) to those of the Eu(III) complexes with model ligands can be explained by the complex composition of the surrounding aqueous matrices and/or additionally binding ligands. Furthermore, the slight differences between the TRLF spectra of Eu(III) species 4 (orange) and 5 (magenta) indicate that, although the binding motif is similar, different organophosphate ligands may bind to Eu(III) inside the cells and in the cell culture medium. Finally, the TRLF spectra

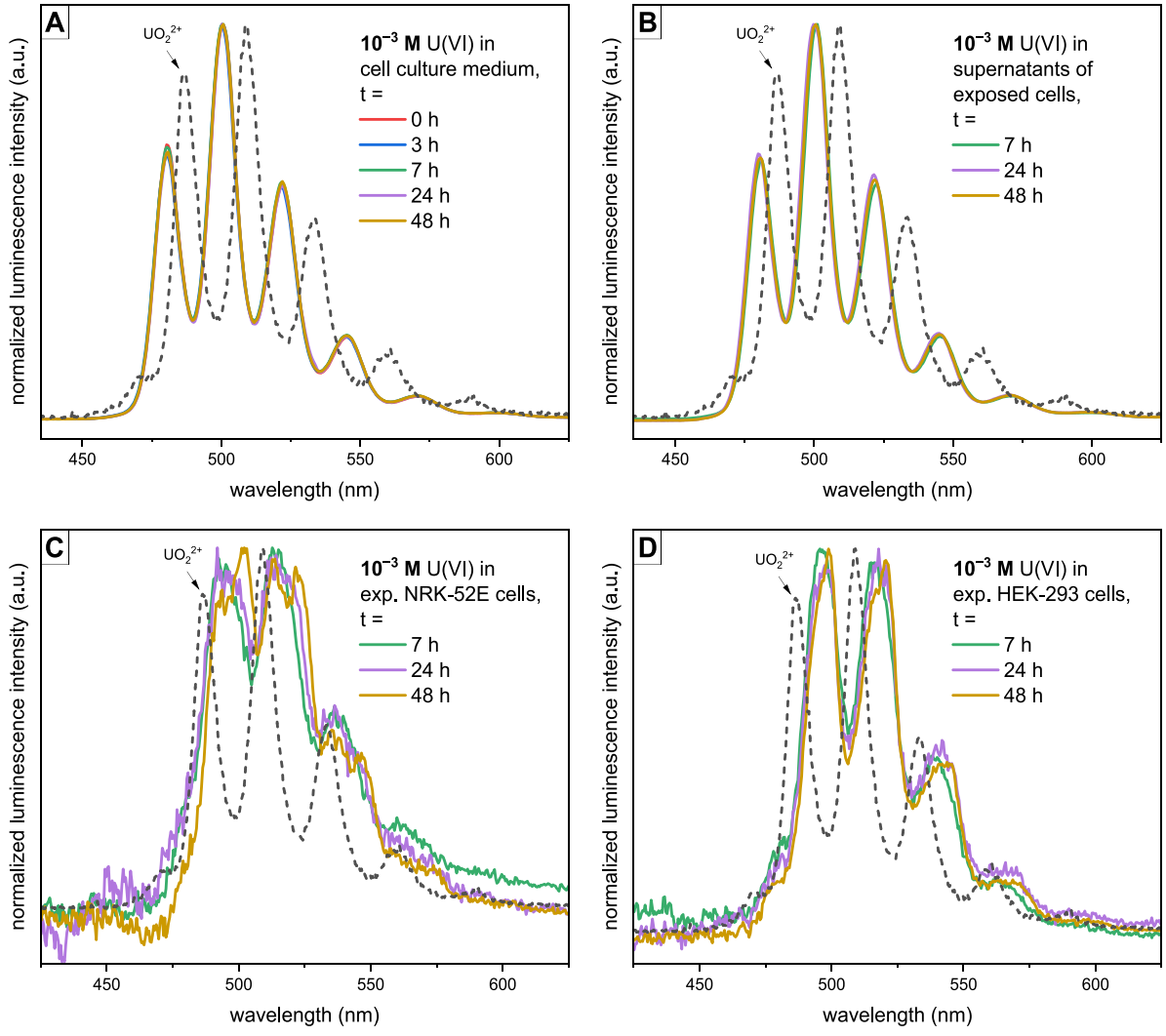

Fig. 10. Steady-state luminescence spectra (0.1 μs delay) of 10^{-3} M U(VI) in cell culture medium (A), in supernatants of exposed cells (B), and in cell suspensions (C, D) after different exposure times. All steady-state spectra were normalized to the band with the highest intensity.

of Eu(III) species 4 (orange) and 5 (magenta) are in very good agreement with those of Eu(III) bound to intracellular organophosphate motifs in winter rye (green species in *Secale cereale* L. (Stadler et al., 2023)) and various fungi (green species in *S. commune*, *P. ostreatus*, *L. tigrinus*, and L. *naucinus* (Günther et al., 2022)).

Comparing the data at 10^{-5} and 10^{-3} M Eu(III), reveals that, in suspensions of exposed cells, only two different binding motifs are found: inorganic and organic phosphate binding sites. In contrast, in cell culture medium and supernatants of exposed cells, an additional protein complex is formed at lower Eu(III) concentration. Although complexation of Eu(III) with organic acids is also very likely in biological fluids, none of the TRLF spectra of the five Eu(III) species exhibited spectroscopic parameters comparable to those of Eu(III) with model organic acid ligands (see ESI, Fig. S7A). Hence, carboxylic acids seem to play, at least, a subordinate role in Eu(III) binding in our cell culture medium and inside rat renal cells (*e.g.,* as second ligand in the ternary Eu(III) species 1 (red) and 2 (green)).

The steady-state spectra of 10^{-3} M U(VI) are shown in Fig. 10 in dependence on the incubation time. Data for 10^{-5} M U(VI) are nearly identical in cell culture medium and supernatants. However, in suspensions of cells exposed to 10^{-5} M U(VI) no spectrum could be recorded. Like for Eu(III), U(VI) spectra in the supernatants of U(VI) exposed NRK-52E cells are nearly identical to those of exposed HEK-293 cells. Therefore, only selected data are shown and discussed in detail. Other data are given in the ESI, Fig. S8, and the spectral parameters are compiled in Table S6 in the ESI. Because the exact quenching mechanism at cryogenic conditions is not fully understood, luminescence lifetimes are not comparable between different cryo-TRLFS systems. However, they are useful to assign species for the same cryo-system.

There are no significant differences between the spectra of U(VI) in cell culture medium and supernatants of exposed cells. Furthermore, there are no spectral alterations over time. Accordingly, the speciation does not change within 48 h. The evaluation of the spectra with PARAFAC shows that only one U(VI) species is formed in both sample sets (see ESI, Fig. S9). In contrast to Eu(III), the proteins of FBS are not involved in U(VI) speciation in the medium, since no differences occur in the spectra of U(VI) in the complete medium and in the medium without FBS (see ESI, Fig. S10). Instead, the band positions as well as the luminescence lifetime agree very well with the $UO_2(CO_3)_3^{4-}$ complex (Fig. S9) (Steudtner et al., 2011). Taking into account the high carbonate concentration of the cell culture medium (44.05 mM) and the pH of 7.4–8.0, this is reasonable. Furthermore, in minimum essential medium (MEM) also a U(VI)-bicarbonate complex is formed despite the lower carbonate concentration of 26.2 mM (Carrière et al., 2006). It is, therefore, assumed that the dominant U(VI) species in DMEM as well as in supernatants of exposed cells is the $UO_2(CO_3)_3^{4-}$ complex or a chemically very similar species. This result is in good agreement with *in vivo* experiments, which proof that U(VI) reaches the proximal tubules epithelium mainly complexed by carbonate or citrate (Carrière et al., 2004).

In cell suspensions exposed to 10^{-3} M U(VI), a luminescence spectrum different from that in cell culture medium was recorded independent from exposure time (Fig. 10C,D). Spectral alterations compared to the cell culture medium are, *e.g.*, red-shift of peaks to higher wavelengths. In comparison, the signal-to-noise ratio of the U(VI) spectrum in the HEK-293 cell suspension is significantly better than that of the NRK-52E cells due to a higher cell density and, hence, presumably a higher amount of adsorbed and/or accumulated U(VI). The splitting of bands (*e.g.*, at 513.2 nm and 521.5 nm) indicates that the luminescence spectra in cell suspensions are composed of two different U(VI) species. Using PARAFAC, the two single component spectra and their distribution were extracted (see ESI, Fig. S9B—D). The first species is the same U(VI)-carbonate complex as found in the cell culture medium (see ESI, Fig. S9C), *i.e.*, presumably an intracellular soluble form of U(VI)-carbonate, which is already described in literature (Carrière et al., 2008). Noteworthy, in suspensions of exposed cells, this species is clearly the minor one (see ESI, Fig. S9B) while it is predominant in cell-free medium. The band positions and luminescence lifetime of the second U(VI) species dominating in suspensions of exposed cells are in good agreement with the reference spectra of U(VI)-HEDP as a model complex for organic U(VI)-phosphate species and inorganic U(VI)-phosphate species (see ESI, Fig. S9D, Bonhoure et al., 2007; Jacopin et al., 2003). Therefore, the second U(VI) is very likely an intracellularly organic or inorganic U(VI)-phosphate species. This is reasonable since U(VI)-phosphate precipitates are found in both NRK-52E and HEK-293 cells by transmission electron microscopy (TEM) and secondary ion mass spectrometry (SIMS) after exposure to 50–500 μM U(VI) (Carrière et al., 2006; Rouas et al., 2010). Furthermore, U(VI) precipitates in LLC-PK_1 kidney cells in the cytoplasmic compartment as U(VI)-phosphate with a needle-like structure (Mirto et al., 1999). For the first time, this U(VI)-phosphate species was now also detected by TRLFS in our study.

In summary, the results of heavy metal speciation in the cell culture medium differ significantly depending on the metal. Ba(II) is predominantly present as free Ba^{2+} ion and Eu(III) forms complexes with (organo-) phosphate(s) and (a) protein(s) from FBS, while U(VI) occurs as carbonate species. Differences in intracellular metal uptake may, therefore, be explained by these variations in speciation. In cell suspension, there are no significant differences between the two cell lines used. In Eu(III) exposed cells, depending on the concentration, one to two species are present having, presumably, an inorganic and/or organic phosphate binding motif. In U(VI) exposed cells, also a phosphatic U(VI) species dominates.

3.6. Intracellular localization and speciation of europium(III)

Chemical microscopy combines luminescence spectroscopic mapping with microscopic imaging and is, therefore, very suitable to determine the spatial distribution and intracellular speciation of Eu(III) within exposed cells.

For chemical microscopy, NRK-52E cells were exposed to $5{\cdot}10^{-4}$ M Eu(III) for 24 h. The overlay of the microscopic image and the Eu(III) luminescence distribution are depicted in Fig. 11A. The respective steady-state luminescence emission spectrum of Eu(III) inside the cells is given in Fig. 11B in comparison to the TRLF spectrum of NRK-52E cells exposed to 10^{-3} M Eu(III) for 24 h.

The luminescence spectroscopic mapping of exposed NRK-52E cells reveals the presence of one prevailing intracellular Eu(III) species, which is mainly localized in granule-like vesicular compartments close to the nucleus. This suggests Eu(III) deposition in the endomembrane transport system with participation, *e.g.*, of the Golgi apparatus. However, differentiation of single cell compartments is not possible in detail with the given microscopic magnification. Nevertheless, Eu(III) associated to the cytoplasmic membrane could not be detected, most likely due to a relatively low percentage of the extracellular binding in comparison to the intracellular accumulation. Thus, chemical microscopy is in good agreement with the conducted ICP-MS analyses, indicating elevated intracellular Eu(III) concentrations after lysis of exposed cells (see Fig. 4).

The Eu(III) steady-state luminescence spectrum of the chemical microscopy with single cells on slides ($\lambda_{exc} = 532$ nm) resembles that of Eu(III) species 1 (red) and 2 (green) measured with TRLFS ($\lambda_{exc} = 394$ nm) in cell suspensions, *i.e.*, Eu(III) bound to inorganic phosphate motif(s). Both spectra exhibit nearly identical overall shape, a weak $^7F_0$ transition and an $R_{E/M}$ of 1.7 (see Fig. 11B and Fig. 8). Pronounced intensity of the $^7F_4$ transition in the Eu(III) spectrum from chemical microscopy can be explained by higher detection sensitivity of the Raman microscope spectrometer in the respective energy range compared to the TRLFS setup and/or different sensitivity and wavelength optimization of the camera systems used for chemical microscopy and TRLFS, respectively. Additional minor peaks in the Eu(III) spectrum from chemical microscopy mainly result from Raman signals of CH_x vibrations (*e.g.*, lipids or carbohydrates from cell compartments) which are not measurable with

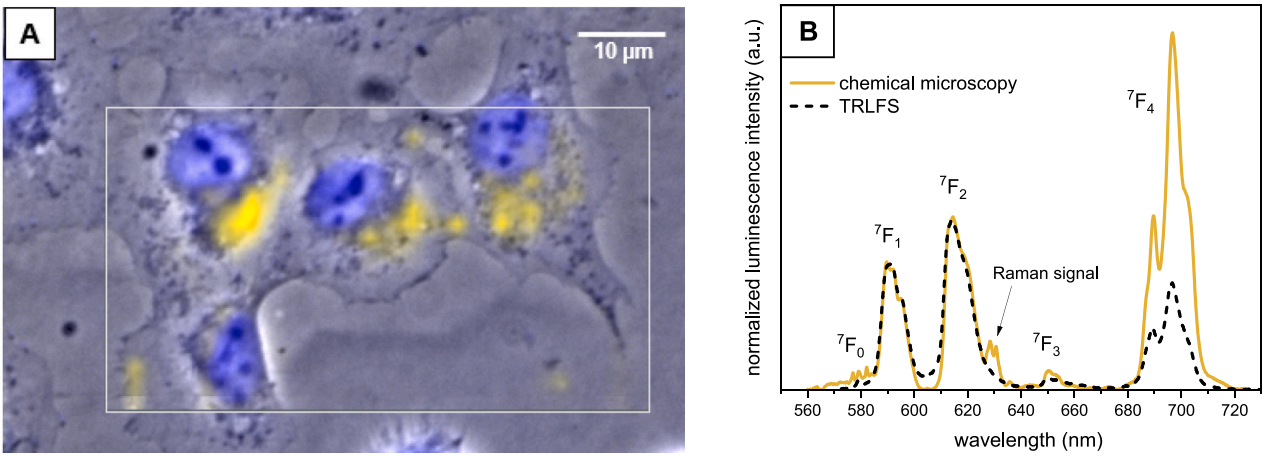

Fig. 11. Chemical microscopy of NRK-52E cells after 24 h exposure to $5{\cdot}10^{-4}$ M Eu(III): (A) Overlay of the Eu(III) species distribution (yellow) within the ROI, DAPI fluorescence of stained nuclei (blue), and phase contrast (grey). Scale bar represents 10 µm and white rectangle is the ROI. (B) Deconvoluted Eu(III) steady-state luminescence spectrum of chemical microscopy (λ_{exc} = 532 nm) compared to TRLFS with NRK-52E cells exposed to 10^{-3} M Eu(III) for 24 h (λ_{exc} = 394 nm; see also Fig. 7).

TRLFS. In conclusion, both methods are suitable to detect the intracellular Eu(III) species and lead to the same speciation results.

Interestingly, based on the spectroscopic characteristics, the Eu(III) binding motif detected in the present study was also found by chemical microscopy in Eu(III) exposed cells of bacterial, plant, and fungi origin (Günther et al., 2022; Hilpmann et al., 2023; Jessat et al., 2023; Klotzsche et al., 2023; Stadler et al., 2023). This indicates Eu(III) complexation by ligands that are ubiquitous in all living organisms. In this regard, inorganic phosphates are a promising candidate, being present in all named species and needed for many cellular key processes or stress responses. Nevertheless, the possibility of a mixed carbonate and/or carboxyl complex cannot be ruled out completely.

Regarding the subcellular localization of Eu(III), a 24 h exposure study on rats indicates accumulation in lysosomes of kidney cells with possible association to endocytic pathways (Bingham and Dobrota, 1994). Lysosomes are acidic organelles (pH 4–5) involved in endocytosis, digestion, and detoxification as well as storage of cellular waste products or non-degradable substrates (Kurz et al., 2008). Other heavy metals like Cd are known to accumulate in lysosomes of kidney cells as well (Chargui et al., 2011). Taking this together, it is conceivable that, in the present study, Eu(III) is taken up by exposed NRK-52E cells *via* endocytosis followed by the formation of intracellular Eu(III)-(organo-) phosphate complexes, and subsequent accumulation in lysosomal compartments. Further investigations verifying this assumption are in progress.

4. Conclusions

In this study, the effect of Ba(II), Eu(III), and U(VI) on cell viability, apoptosis/necrosis, and intracellular uptake as well as their speciation in rat NRK-52E and human HEK-293 kidney cells was investigated. For Ba(II), neither cytotoxic effects nor enhanced cell death were detected in both cell lines even after 48 h exposure to 10^{-3} M. In addition, the amount of Ba(II) taken up by the cells was very low and independent from the exposure time. In contrast to that, for Eu(III) and U(VI), both cell viability and intracellular metal uptake are clearly time- and concentration-dependent. Thereby, U(VI) exhibits a significantly higher cytotoxicity and a higher accumulation in both cell lines than Eu(III). Furthermore, 24 h exposure to 10^{-3} M heavy metal induces apoptotic effects in the case of Eu(III), whereas necrotic and presumably pyroptotic cell death dominate in the case of U(VI). Hence, the correlation between intracellular metal uptake and cell viability found in this study suggests that the cytotoxicity of metals strongly depends on their intracellular uptake and the elements rank in the following order: Ba(II) << Eu(III) < U(VI).

In case of all three heavy metals, no adverse effects on human and rat kidney cells were detected at environmental concentrations in surface waters which typically are in the range of 10–60 µg/L for Ba(II) ($7.3{\cdot}10^{-8}$–$4.4{\cdot}10^{-7}$ M) (Oskarsson, 2015; Poddalgoda et al., 2017), 0.0002–0.07 µg/L for Eu(III) ($1.3{\cdot}10^{-12}$–$4.6{\cdot}10^{-10}$ M) (Kulaksız and Bau, 2013; Négrel et al., 2000), and < 4 µg/L for U(VI) (<$1.7{\cdot}10^{-8}$ M) (Smedley and Kinniburgh, 2023), respectively. However, at elevated concentrations potentially occurring in uranium mining areas (Wang et al., 2012), U(VI) exhibits a harmful effect onto kidney cells already after short-time exposure for 7 h, which increases with prolonged exposure time. The remarkable non-cytotoxicity of Ba(II) even at millimolar concentrations, in turn, is quite surprising since it is known as an environmental toxicological agent and severe renal damage after Ba(II) exposure is described in the literature (Ananda et al., 2013; Dietz et al., 1992; Mohammed and Ismail, 2017; Wetherill et al., 1981). Comparing both kidney cell lines reveals that rat NRK-52E cells seem to be more susceptible to Eu(III) and U(VI) cytotoxicity than human HEK-293 cells underlining the importance of experiments with human cells for the risk assessment of heavy metals in the human organism.

Speciation studies using TRLFS reveal that Eu(III) is bound dominantly to (organo-) phosphate motifs as well as to a protein of FBS in cell culture medium and supernatants of exposed cells whereas, in suspension of both exposed NRK-52E and HEK-293 cells, only Eu(III) species with (organo-) phosphate binding motifs are formed. U(VI), on the other hand, forms a soluble carbonate species in cell culture medium whereas, in exposed cell suspensions, both a U(VI)-carbonate and a U(VI)-phosphate species are formed. This verifies the hypothesis of Carrière et al. (2008) that U(VI) is taken up into the kidney cells as a soluble carbonate species and, then, partially precipitates as U(VI)-phosphate in the lysosomes while the remaining U(VI) is found as a carbonate species inside the cells. Additionally, these authors suggested that U(VI) phosphate is taken up into cells in soluble or precipitated form. This could not be proven within this study, since there are no indications for an U(VI)-phosphate complex in cell-free medium.

For the first time, the combination of microscopy and luminescence spectroscopy enabled to study the intracellular distribution and speciation of Eu(III) in NRK-52E cells. We demonstrated that Eu(III) accumulates mainly near the nucleus in granular-like vesicular compartments and forms the same phosphatic Eu(III) species as in the cell suspensions measured by TRLFS. This study, thus, highlights the importance of combining microscopic, analytical, and spectroscopic methods with *in vitro* cell culture experiments and helps to improve the risk assessment not only for Ba(II), Eu(III), and U(VI) themselves but also

for the radioactive Ba(II)- and Eu(III)-analogs Ra(II) and Cm/Am(III), respectively.

Funding

This work was funded by the German Federal Ministry of Education and Research (BMBF) under grant numbers 02NUK057A and 02NUK057B and is part of the joint project RADEKOR. L.H. acknowledges funding received from BMBF under grant number 02NUK057D.

CRediT authorship contribution statement

Christian Senwitz: Writing – original draft, Visualization, Methodology, Investigation, Formal analysis. **Daniel Butscher:** Writing – original draft, Visualization, Methodology, Investigation, Formal analysis. **Linus Holtmann:** Writing – review & editing, Visualization, Investigation, Formal analysis. **Manja Vogel:** Writing – review & editing, Visualization, Investigation, Formal analysis. **Robin Steudtner:** Writing – review & editing, Visualization, Formal analysis. **Björn Drobot:** Writing – review & editing, Visualization, Formal analysis. **Thorsten Stumpf:** Writing – review & editing, Supervision. **Astrid Barkleit:** Writing – review & editing, Supervision, Project administration, Funding acquisition, Conceptualization. **Anne Heller:** Writing – review & editing, Visualization, Supervision, Project administration, Methodology, Investigation, Funding acquisition, Formal analysis, Conceptualization.

Declaration of competing interest

The authors declare that they have no known competing financial interests or personal relationships that could have appeared to influence the work reported in this paper.

Data availability

Data will be made available on request.

Acknowledgement

The authors thank Stefanie Rebisch from Technische Universität Dresden, Chair of Radiochemistry and Radioecology for her valuable support in cell culture experiments as well as Stephan Weiß and Sabrina Beutner from Helmholtz-Zentrum Dresden-Rossendorf, Institute of Resource Ecology for their assistance with the ultracentrifugation and performing ICP-MS measurements, respectively. Finally, the authors kindly thank Margret Acker, Steffen Taut, and the staff from the Central Radionuclide Laboratory of the Technische Universität Dresden for the possibility to conduct most part of the work in their labs as well as for their valuable support and discussions.

Appendix A. Supplementary data

The following supporting information can be downloaded: Tab. S1: cell culture medium composition, Fig. S1: dose-response-curves of U(VI) in DMEM w/o pyruvate, Tab. S2: EC_{50} values and cell viabilities for U (VI) exposed NRK-52E cells in DMEM w/o pyruvate, Fig. S2: growth curves of HEK-293 and NRK-52E cells, Tab. S3 + Fig. S3: intracellular metal uptake of Ba(II), Eu(III), and U(VI), Fig. S4: intracellular U(VI) uptake with HEDP as washing agent, Fig. S5: thermodynamic modelling of Ba(II) speciation in cell culture medium, Tab. S4: Ba(II) solubility in different mixtures of inorganic salts from cell culture medium, Tab. S5 + Fig. S6: TRLFS parameter and spectra for Eu(III) in cell culture medium, supernatants, and exposed cell suspensions, Fig. S7: PARAFAC results for 10^{-5} M Eu(III) TRLFS, Fig. S8 + Tab. S6: TRLFS parameter and spectra for U(VI) in cell culture medium, supernatants, and exposed cell suspensions, Fig. S9 + S10: TRLFS reference spectra for U(VI). Supplementary data to this article can be found online at https://doi.org/10.1016/j.scitotenv.2024.171374.

References

Akbar, M.U., Ahmad, M.R., Shaheen, A., Mushtaq, S., 2016. A review on evaluation of technetium-99m labeled radiopharmaceuticals. J. Radioanal. Nucl. Chem. 310, 477–493. https://doi.org/10.1007/s10967-016-5019-7.

Alfadda, A.A., Sallam, R.M., 2012. Reactive oxygen species in health and disease. J. Biomed. Biotechnol. 2012 https://doi.org/10.1155/2012/936486.

Ananda, S., Shaohua, Z., Liang, L., 2013. Fatal barium chloride poisoning: four cases report and literature review. Am. J. Forensic Med. Pathol. 34, 115–118. https://doi.org/10.1097/PAF.0b013e31828a2626.

Ansoborlo, E., Adam-Guillermin, C., 2012. Radionuclide transfer processes in the biosphere. Radionucl. Behav. Nat. Environ. Sci. Implic. Lessons Nucl. Ind. 484–513. https://doi.org/10.1533/9780857097194.2.484.

Ansoborlo, E., Prat, O., Moisy, P., Den Auwer, C., Guilbaud, P., Carriere, M., Gouget, B., Duffield, J., Doizi, D., Vercouter, T., Moulin, C., Moulin, V., 2006. Actinide speciation in relation to biological processes. Biochimie 88, 1605–1618. https://doi.org/10.1016/j.biochi.2006.06.011.

Bao, Y., Wang, D., Li, Z., Hu, Y., Xu, A., Wang, Q., Shao, C., Chen, H., 2013. Efficacy of a novel chelator BPCBG for removing uranium and protecting against uranium-induced renal cell damage in rats and HK-2 cells. Toxicol. Appl. Pharmacol. 269, 17–24. https://doi.org/10.1016/j.taap.2013.02.010.

Barkleit, A., Wilke, C., Heller, A., Stumpf, T., Ikeda-ohno, A., 2017. Trivalent f-elements in human saliva: a comprehensive speciation study by time-resolved laser-induced fluorescence spectroscopy and thermodynamic calculations. Dalt. Trans. 46, 1593–1605. https://doi.org/10.1039/c6dt03726g.

Bingham, D., Dobrota, M., 1994. Distribution and excretion of lanthanides: comparison between europium salts and complexes. Biometals 7, 142–148. https://doi.org/10.1007/BF00140484.

Blount, C.W., 1977. Barite solubilities and thermodynamic quantities up to 300 degrees C and 1400 bars. Am. Mineral. 62, 942–957.

Bonhoure, I., Meca, S., Marti, V., De Pablo, J., Cortina, J.L., 2007. A new time-resolved laser-induced fluorescence spectrometry (TRLFS) data acquisition procedure applied to the uranyl-phosphate system. Radiochim. Acta 95, 165–172. https://doi.org/10.1524/ract.2007.95.3.165.

Busenberg, E., Plummer, L.N., 1986. The solubility of $BaCO_3$(cr) (witherite) in CO_2-H_2O solutions between 0 and 90°C, evaluation of the association constants of $BaHCO_3^+$(aq) and $BaCO_3^0$(aq) between 5 and 80°C, and a preliminary evaluation of the thermodynamic properties of Ba^{2+}(aq). Geochim. Cosmochim. Acta 50, 2225–2233. https://doi.org/10.1016/0016-7037(86)90077-3.

Carrière, M., Avoscan, L., Collins, R., Carrot, F., Khodja, H., Ansoborlo, E., Gouget, B., 2004. Influence of uranium speciation on normal rat kidney (NRK-52E) proximal cell cytotoxicity. Chem. Res. Toxicol. 17, 446–452. https://doi.org/10.1021/tx034224h.

Carrière, M., Gouget, B., Gallien, J.P., Avoscan, L., Gobin, R., Verbavatz, J.M., Khodja, H., 2005a. Cellular distribution of uranium after acute exposure of renal epithelial cells: SEM, TEM and nuclear microscopy analysis. Nucl. Instruments Methods Phys. Res. Sect. B Beam Interact. with Mater. Atoms 231, 268–273. https://doi.org/10.1016/j.nimb.2005.01.069.

Carrière, M., Khodja, H., Avoscan, L., Carrot, F., Gouget, B., 2005b. Uranium(VI) complexation in cell culture medium: influence of speciation on normal rat kidney (NRK-52E) cell accumulation. Radiochim. Acta 93, 691–697. https://doi.org/10.1524/ract.2005.93.11.691.

Carrière, M., Thiebault, C., Milgram, S., Avoscan, L., Proux, O., Gouget, B., 2006. Citrate does not change uranium chemical speciation in cell culture medium but increases its toxicity and accumulation in NRK-52E cells. Chem. Res. Toxicol. 19, 1637–1642. https://doi.org/10.1021/tx060206z.

Carrière, M., Proux, O., Milgram, S., Thiebault, C., Avoscan, L., Barre, N., Den Auwer, C., Gouget, B., 2008. Transmission electron microscopic and X-ray absorption fine structure spectroscopic investigation of U repartition and speciation after accumulation in renal cells. J. Biol. Inorg. Chem. 13, 655–662. https://doi.org/10.1007/s00775-008-0350-2.

Chargui, A., Zekri, S., Jacquillet, G., Rubera, I., Ilie, M., Belaid, A., Duranton, C., Tauc, M., Hofman, P., Poujeol, P., El May, M.V., Mograbi, B., 2011. Cadmium-induced autophagy in rat kidney: An early biomarker of subtoxic exposure. Toxicol. Sci. 121, 31–42. https://doi.org/10.1093/toxsci/kfr031.

Chen, B., Hong, S., Dai, X., Li, X., Huang, Q., Sun, T., Cao, D., Zhang, H., Chai, Z., Diwu, J., Wang, S., 2022. In vivo uranium decorporation by a tailor-made hexadentate ligand. J. Am. Chem. Soc. 144, 11054–11058. https://doi.org/10.1021/jacs.2c00688.

Cheng, Y., Liu, M., Li, R., Wang, C., Bai, C., Wang, K., 1999. Gadolinium induces domain and pore formation of human erythrocyte membrane: an atomic force microscopic study. Biochim. Biophys. Acta Biomembr. 1421, 249–260. https://doi.org/10.1016/S0005-2736(99)00125-X.

Cheng, X., Chu, J., Zhang, L., Suo, Z., Tang, W., 2022. Intracellular and extracellular untargeted metabolomics reveal the effect of acute uranium exposure in HK-2 cells. Toxicology 473, 153196. https://doi.org/10.1016/J.TOX.2022.153196.

Concha, N.O., Head, J.F., Kaetzel, M.A., Dedman, J.R., Seaton, B.A., 1992. Annexin V forms calcium-dependent trimeric units on phospholipid vesicles. FEBS Lett. 314, 159–162. https://doi.org/10.1016/0014-5793(92)80964-I.

Dallas, C.E., Williams, P.L., 2001. Barium: rationale for a new oral reference dose. J. Toxicol. Environ. Heal. - Part B Crit. Rev. 4, 395–429. https://doi.org/10.1080/109374001753146216.

De Larco, J.E., Todaro, G.J., 1978. Growth factors from murine sarcoma virus-transformed cells. Proc. Natl. Acad. Sci. U. S. A. 75, 4001–4005. https://doi.org/10.1073/pnas.75.8.4001.

Dietz, D.D., Elwell, M.R., Davis, W.E., Meirhenry, E.F., 1992. Subchronic toxicity of barium chloride dihydrate administered to rats and mice in the drinking water. Toxicol. Sci. 19, 527–537. https://doi.org/10.1093/toxsci/19.4.527.

Domínguez, C., Solé, E., Fortuny, A., 2002. In vitro lead-induced cell toxicity and cytoprotective activity of fetal calf serum in human fibroblasts. Mol. Cell. Biochem. 237, 47–53. https://doi.org/10.1023/A:1016547519763.

Drobot, B., Steudtner, R., Raff, J., Geipel, G., Brendler, V., Tsushima, S., 2015. Combining luminescence spectroscopy, parallel factor analysis and quantum chemistry to reveal metal speciation - a case study of uranyl(VI) hydrolysis. Chem. Sci. 6, 964–972. https://doi.org/10.1039/c4sc02022g.

Drobot, B., Schmidt, M., Mochizuki, Y., Abe, T., Okuwaki, K., Brulfert, F., Falke, S., Samsonov, S.A., Komeiji, Y., Betzel, C., Stumpf, T., Raff, J., Tsushima, S., 2019. Cm^{3+}/Eu^{3+} induced structural, mechanistic and functional implications for calmodulin. Phys. Chem. Chem. Phys. 21, 21213–21222. https://doi.org/10.1039/c9cp03750k.

Du, X.L., Zhang, T.L., Yuan, L., Zhao, Y.Y., Li, R.C., Wang, K., Yan, S.C., Zhang, L., Sun, H., Qian, Z.M., 2002. Complexation of ytterbium to human transferrin and its uptake by K562 cells. Eur. J. Biochem. 269, 6082–6090. https://doi.org/10.1046/j.1432-1033.2002.03326.x.

Elwej, A., Ben Salah, G., Kallel, C., Fakhfakh, F., Zeghal, N., Ben Amara, I., 2016. Protective effects of pomegranate peel against hematotoxicity, chromosomal aberrations, and genotoxicity induced by barium chloride in adult rats. Pharm. Biol. 54, 964–974. https://doi.org/10.3109/13880209.2015.1087035.

Elwej, A., Ghorbel, I., Chaabane, M., Soudani, N., Marrekchi, R., Jamoussi, K., Mnif, H., Boudawara, T., Zeghal, N., Sefi, M., 2017. Protective effects of dietary selenium and vitamin C in barium-induced cardiotoxicity. Hum. Exp. Toxicol. 36, 1146–1157. https://doi.org/10.1177/0960327116681651.

Fattal, E., Tsapis, N., Phan, G., 2015. Novel drug delivery systems for actinides (uranium and plutonium) decontamination agents. Adv. Drug Deliv. Rev. 90, 40–54. https://doi.org/10.1016/j.addr.2015.06.009.

Felmy, A.R., Rai, D., Amonette, J.E., 1990. The solubility of barite and celestite in sodium sulfate: evaluation of thermodynamic data. J. Solution Chem. 19, 175–185. https://doi.org/10.1007/BF00646611.

Fink, S.L., Cookson, B.T., 2005. Apoptosis, pyroptosis, and necrosis: mechanistic description of dead and dying eukaryotic cells. Infect. Immun. 73, 1907–1916. https://doi.org/10.1128/IAI.73.4.1907-1916.2005.

Giffaut, E., Grivé, M., Blanc, P., Vieillard, P., Colàs, E., Gailhanou, H., Gaboreau, S., Marty, N., Madé, B., Duro, L., 2014. Andra thermodynamic database for performance assessment: ThermoChimie. Appl. Geochemistry 49, 225–236. https://doi.org/10.1016/j.apgeochem.2014.05.007.

Graham, F.L., Smiley, J., Russell, W.C., Nairn, R., 1977. Characteristics of a human cell line transformed by DNA from human adenovirus type 5. J. Gen. Virol. 36, 59–72. https://doi.org/10.1099/0022-1317-36-1-59.

Grubbs, F.E., 1969. Procedures for detecting outlying observations in samples. Technometrics 11, 1–21. https://doi.org/10.1080/00401706.1969.10490657.

Gudelis, A., Gorina, I., 2015. On release of radionuclides from a near-surface radioactive waste repository to the environment. Nukleonika 60, 551–555. https://doi.org/10.1515/nuka-2015-0091.

Günther, A., Wollenberg, A., Vogel, M., Drobot, B., Steudtner, R., Freitag, L., Hübner, R., Stumpf, T., Raff, J., 2022. Speciation and spatial distribution of Eu(III) in fungal mycelium. Sci. Total Environ. 851 https://doi.org/10.1016/j.scitotenv.2022.158160.

Haase, H., Hebel, S., Engelhardt, G., Rink, L., 2015. The biochemical effects of extracellular Zn^{2+} and other metal ions are severely affected by their speciation in cell culture media. Metallomics 7, 97–106. https://doi.org/10.1039/c4mt00206g.

Hao, Y., Ren, J., Liu, C., Li, H., Liu, J., Yang, Z., Li, R., Su, Y., 2014. Zinc protects human kidney cells from depleted uranium-induced apoptosis. Basic Clin. Pharmacol. Toxicol. 114, 271–280. https://doi.org/10.1111/bcpt.12167.

Heller, A., Barkleit, A., Bernhard, G., 2011. Chemical speciation of trivalent actinides and lanthanides in biological fluids: the dominant in vitro binding form of curium(III) and europium(III) in human urine. Chem. Res. Toxicol. 24, 193–203. https://doi.org/10.1021/tx100273g.

Heller, A., Barkleit, A., Bok, F., Wober, J., 2019. Effect of four lanthanides onto the viability of two mammalian kidney cell lines. Ecotoxicol. Environ. Saf. 173, 469–481. https://doi.org/10.1016/j.ecoenv.2019.02.013.

Heller, A., Pisarevskaja, A., Bölicke, N., Barkleit, A., Bok, F., Wober, J., 2021. The effect of four lanthanides onto a rat kidney cell line (NRK-52E) is dependent on the composition of the cell culture medium. Toxicology 456. https://doi.org/10.1016/j.tox.2021.152771.

Henge-Napoli, M.H., Ansoborlo, E., Chazel, V., Houpert, P., Paquet, F., Gourmelon, P., 1999. Efficacy of ethane-1-hydroxy-1,1-bisphosphonate (EHBP) for the decorporation of uranium after intramuscular contamination in rats. Int. J. Radiat. Biol. 75, 1473–1477. https://doi.org/10.1080/095530099139331.

Hilpmann, S., Moll, H., Drobot, B., Vogel, M., Hübner, R., Stumpf, T., Cherkouk, A., 2023. Europium(III) as luminescence probe for interactions of a sulfate-reducing microorganism with potentially toxic metals. Ecotoxicol. Environ. Saf. 264 https://doi.org/10.1016/j.ecoenv.2023.115474.

Huang, L., Sun, G., Xu, W., Li, S., Qin, X., An, Q., Wang, Z., Li, J., 2023. Uranium uptake is mediated markedly by clathrin-mediated endocytosis and induce dose-dependent toxicity in HK-2 cells. Environ. Toxicol. Pharmacol. 101, 104171 https://doi.org/10.1016/j.etap.2023.104171.

ICRP, 1995. ICRP Publication 69: Age-dependent doses to members of the public from intake of radionuclides: Part 3 ingestion dose coefficients. Elsevier Heal. Sci. https://doi.org/10.1016/0146-6453(81)90127-5.

Jacopin, C., Sawicki, M., Plancque, G., Doizi, D., Ansoborlo, E., Amekraz, B., Moulin, C., 2003. Investigation of the interaction between 1-Hydroxyethane-1, 1′-diphosphonic acid (HEDP) and uranium (VI). Inorg. Chem. 42, 5015–5022.

Jessat, J., Moll, H., John, W.A., Bilke, M.L., Hübner, R., Kretzschmar, J., Steudtner, R., Drobot, B., Stumpf, T., Sachs, S., 2022. A comprehensive study on the interaction of Eu(III) and U(VI) with plant cells (Daucus carota) in suspension. J. Hazard. Mater. 439 https://doi.org/10.1016/j.jhazmat.2022.129520.

Jessat, J., John, W.A., Moll, H., Vogel, M., Steudtner, R., Drobot, B., Hübner, R., Stumpf, T., Sachs, S., 2023. Localization and chemical speciation of europium(III) in Brassica napus plants. Ecotoxicol. Environ. Saf. 254 https://doi.org/10.1016/j.ecoenv.2023.114741.

Kajjumba, G.W., Attene-Ramos, M., Marti, E.J., 2021. Toxicity of lanthanide coagulants assessed using four in vitro bioassays. Sci. Total Environ. 800, 149556 https://doi.org/10.1016/j.scitotenv.2021.149556.

Kimura, T., Kato, Y., 1998. Luminescence study on hydration states of lanthanide(III)-polyaminopolycarboxylate complexes in aqueous solution. J. Alloys Compd. 275–277, 806–810. https://doi.org/10.1016/S0925-8388(98)00446-0.

Kinniburgh, D., Cooper, D., 2011. PhreePlot: Creating Graphical Output with PHREEQC [WWW Document].

Klotzsche, M., Vogel, M., Sachs, S., Raff, J., Stumpf, T., Drobot, B., Steudtner, R., 2023. How tobacco (Nicotiana tabacum) BY-2 cells cope with Eu(III) - a microspectroscopic study. Analyst 148. https://doi.org/10.1039/d3an00741c.

Kovacs, S.B., Miao, E.A., 2017. Gasdermins: effectors of Pyroptosis. Trends Cell Biol. 27, 673–684. https://doi.org/10.1016/j.tcb.2017.05.005.

Krishna, S., Jaiswal, A., Sujata M., Gupta, Sharma, D., Ali, Z., 2020. Barium poisoning with analytical aspects and its management. Int. J. Adv. Res. Med. Chem. 2, 20–27.

Kulaksız, S., Bau, M., 2013. Anthropogenic dissolved and colloid/nanoparticle-bound samarium, lanthanum and gadolinium in the Rhine River and the impending destruction of the natural rare earth element distribution in rivers. Earth Planet. Sci. Lett. 362, 43–50. https://doi.org/10.1016/j.epsl.2012.11.033.

Kurz, T., Terman, A., Gustafsson, B., Brunk, U.T., 2008. Lysosomes and oxidative stress in aging and apoptosis. Biochim. Biophys. Acta - Gen. Subj. 1780, 1291–1303. https://doi.org/10.1016/j.bbagen.2008.01.009.

Lawal, A.O., Ellis, E., 2010. Differential sensitivity and responsiveness of three human cell lines HepG2, 1321N1 and HEK 293 to cadmium. J. Toxicol. Sci. 35, 465–478. https://doi.org/10.2131/jts.35.465.

Lee, W.K., Probst, S., Santoyo-Sánchez, M.P., Al-Hamdani, W., Diebels, I., von Sivers, J. K., Kerek, E., Prenner, E.J., Thévenod, F., 2017. Initial autophagic protection switches to disruption of autophagic flux by lysosomal instability during cadmium stress accrual in renal NRK-52E cells. Arch. Toxicol. 91, 3225–3245. https://doi.org/10.1007/s00204-017-1942-9.

Lee, D.Y., Lee, S.Y., Yun, S.H., Jeong, J.W., Kim, J.H., Kim, H.W., Choi, J.S., Kim, G.D., Joo, S.T., Choi, I., Hur, S.J., 2022. Review of the current research on fetal bovine serum and the development of cultured meat. Food Sci. Anim. Resour. 42, 775–799. https://doi.org/10.5851/kosfa.2022.e46.

Leggett, R., Ansoborlo, E., Bailey, M., Gregoratto, D., Paquet, F., Taylor, D., 2014. Biokinetic data and models for occupational intake of lanthanoids. Int. J. Radiat. Biol. 90, 996–1010. https://doi.org/10.3109/09553002.2014.887868.

Lipsztein, J.L., Dias da Cunha, K.M., Azeredo, A.M.G., Julião, L., Santos, M., Melo, D.R., Simões Filho, F.F.L., 2001. Exposure of workers in mineral processing industries in Brazil. J. Environ. Radioact. 54, 189–199. https://doi.org/10.1016/S0265-931X(00)00174-0.

Liu, H., Yuan, L., Yang, X., Wang, K., 2003. La^{3+}, Gd^{3+} and Yb^{3+} induced changes in mitochondrial structure, membrane permeability, cytochrome c release and intracellular ROS level. Chem. Biol. Interact. 146, 27–37. https://doi.org/10.1016/S0009-2797(03)00072-3.

Liu, J., Li, N., Ma, L., Duan, Y., Wang, J., Zhao, X., Wang, S., Wang, H., Hong, F., 2010. Oxidative injury in the mouse spleen caused by lanthanides. J. Alloys Compd. 489, 708–713. https://doi.org/10.1016/j.jallcom.2009.09.158.

Machata, G., 1988. Barium. In: Seiler, H.G., Sigel, H., Sigel, A. (Eds.), Handbook on Toxicity of Inorganic Compounds. New York.

Martínez, A.B., Cabrini, R.L., Ubios, A.M., 2000. Orally administered ethane-1-hydroxy-1,1-biphosphonate reduces the lethal effect of oral uranium poisoning. Health Phys. 78, 668–671. https://doi.org/10.1097/00004032-200006000-00009.

Milgram, S., Carrière, M., Thiebault, C., Berger, P., Khodja, H., Gouget, B., 2007. Cell-metal interactions: a comparison of natural uranium to other common metals in renal cells and bone osteoblasts. Nucl. Instruments Methods Phys. Res. Sect. B Beam Interact. with Mater. Atoms 260, 254–258. https://doi.org/10.1016/j.nimb.2007.02.030.

Milgram, S., Carrière, M., Thiebault, C., Malaval, L., Gouget, B., 2008. Cytotoxic and phenotypic effects of uranium and lead on osteoblastic cells are highly dependent on metal speciation. Toxicology 250, 62–69. https://doi.org/10.1016/j.tox.2008.06.003.

Mirto, H., Hengé-Napoli, M.H., Gibert, R., Ansoborlo, E., Fournier, M., Cambar, J., 1999. Intracellular behaviour of uranium(VI) on renal epithelial cell in culture (LLC-PK1): influence of uranium speciation. Toxicol. Lett. 104, 249–256. https://doi.org/10.1016/S0378-4274(98)00371-3.

Mohammed, A.T., Ismail, H.T.H., 2017. Hematological, biochemical, and histopathological impacts of barium chloride and barium carbonate accumulation in soft tissues of male Sprague-Dawley rats. Environ. Sci. Pollut. Res. 24, 26634–26645. https://doi.org/10.1007/s11356-017-0282-x.

Muller, D., Houpert, P., Cambar, J., Hengé-Napoli, M.H., 2006. Role of the sodium-dependent phosphate co-transporters and of the phosphate complexes of uranyl in the cytotoxicity of uranium in LLC-PK1 cells. Toxicol. Appl. Pharmacol. 214, 166–177. https://doi.org/10.1016/j.taap.2005.12.016.

Muller, D.S., Houpert, P., Cambar, J., Hengé-Napoli, M.H., 2008. Role of the sodium-dependent phosphate cotransporters and absorptive endocytosis in the uptake of low concentrations of uranium and its toxicity at higher concentrations in LLC-PK1 cells. Toxicol. Sci. 101, 254–262. https://doi.org/10.1093/toxsci/kfm266.

Négrel, P., Guerrot, C., Cocherie, A., Azaroual, M., Brach, M., Fouillac, C., 2000. Rare earth elements, neodymium and strontium isotopic systematics in mineral waters: evidence from the Massif Central, France. Appl. Geochemistry 15, 1345–1367. https://doi.org/10.1016/S0883-2927(00)00008-1.

Omole, J.G., Alabi, Q.K., Aturamu, A., Adefisayo, M.A., Oluwayomi, O., Dada, M.B., Ige, M.S., 2019. Barium chloride dose-dependently induced heart and lung injury in Wistar rats. Environ. Toxicol. 34, 1303–1312. https://doi.org/10.1002/tox.22831.

Oskarsson, A., 2015. Barium. In: Nordberg, G.F., Fowler, B.A., Nordberg, M. (Eds.), Handbook on the Toxicology of Metals: Fourth Edition. Academic Press, pp. 625–634. https://doi.org/10.1016/B978-0-444-59453-2.00029-9.

Pałasz, A., Segovia, Y., Skowronek, R., Worthington, J.J., 2019. Molecular neurochemistry of the lanthanides. Synapse 73, 1–14. https://doi.org/10.1002/syn.22119.

Pallares, R.M., Panyala, N.R., Sturzbecher-Hoehne, M., Illy, M.C., Abergel, R.J., 2020. Characterizing the general chelating affinity of serum protein fetuin for lanthanides. J. Biol. Inorg. Chem. 25, 941–948. https://doi.org/10.1007/s00775-020-01815-x.

Panak, P., Selenska-Pobell, S., Kutschke, S., Geipel, G., Bernhard, G., Nitsche, H., 1999. Complexation of U(VI) with cells of Thiobacillus ferrooxidans and Thiomonas cuprina of different geological origin. Radiochim. Acta 84, 183–190. https://doi.org/10.1524/ract.1999.84.4.183.

Parkhurst, D.L., Appelo, C.A.J., 2013. Description of input and examples for PHREEQC version 3—A computer program for speciation, batch-reaction, one-dimensional transport, and inverse geochemical valculations. In: Modeling Techniques. U.S. Geological Survey.

Plum, L.M., Rink, L., Hajo, H., 2010. The essential toxin: impact of zinc on human health. Int. J. Environ. Res. Public Health 7, 1342–1365. https://doi.org/10.3390/ijerph7041342.

Poddalgoda, D., Macey, K., Assad, H., Krishnan, K., 2017. Development of biomonitoring equivalents for barium in urine and plasma for interpreting human biomonitoring data. Regul. Toxicol. Pharmacol. 86, 303–311. https://doi.org/10.1016/j.yrtph.2017.03.022.

Prat, O., Berenguer, F., Malard, V., Tavan, E., Sage, N., Steinmetz, G., Quemeneur, E., 2005. Transcriptomic and proteomic responses of human renal HEK293 cells to uranium toxicity. Proteomics 5, 297–306. https://doi.org/10.1002/pmic.200400896.

Reeves, J.P., Condrescu, M., 2003. Lanthanum is transported by the sodium/calcium exchanger and regulates its activity. Am. J. Physiol. - Cell Physiol. 285, 763–770. https://doi.org/10.1152/ajpcell.00168.2003.

Rim, K.T., Koo, K.H., Park, J.S., 2013. Toxicological evaluations of rare earths and their health impacts to workers: a literature review. Saf. Health Work 4, 12–26. https://doi.org/10.5491/SHAW.2013.4.1.12.

Rohde, F., Braumann, U.D., Schmidt, M., 2020. Correlia: an ImageJ plug-in to co-register and visualise multimodal correlative micrographs. J. Microsc. 280, 3–11. https://doi.org/10.1111/jmi.12928.

Romanov, S.A., Efimov, V.V., Aladova G.G., Suslova, Kuznetsova, I.S., Sokolova V. V., Khokhryakov, Sypko, S.A., Ishunina, M.V., Khokhryakov, V.F., 2020. Plutonium production and particles incorporation into the human body. J. Environ. Radioact. 211, 106073 https://doi.org/10.1016/j.jenvrad.2019.106073.

Romero, P.J., Romero, E.A., 1999. Effect of cell ageing on Ca^{2+} influx into human red cells. Cell Calcium 26, 131–137. https://doi.org/10.1054/ceca.1999.0063.

Rouas, C., Bensoussan, H., Suhard, D., Tessier, C., Grandcolas, L., Rebiere, F., Dublineau, I., Taouis, M., Pallardy, M., Lestaevel, P., Gueguen, Y., 2010. Distribution of soluble uranium in the nuclear cell compartment at subtoxic concentrations. Chem. Res. Toxicol. 23, 1883–1889. https://doi.org/10.1021/tx100168c.

Roza, O., Berman, L.B., 1971. The pathophysiology of barium: hypokalemic and cardiovascular effects. J. Pharmacol. Exp. Ther. 177, 433–439. https://doi.org/10.1136/jnnp.37.1.32.

Sachs, S., Heller, A., Weiss, S., Bok, F., Bernhard, G., 2015. Interaction of Eu(III) with mammalian cells: cytotoxicity, uptake, and speciation as a function of Eu(III) concentration and nutrient composition. Toxicol. Vitr. 29, 1555–1568. https://doi.org/10.1016/j.tiv.2015.06.006.

Schott, G.D., McArdle, B., 1974. Barium induced skeletal muscle paralysis in the rat, and its relationship to human familial periodic paralysis. J. Neurol. Neurosurg. Psychiatry 37, 32–39. https://doi.org/10.1136/jnnp.37.1.32.

Scudiero, D.A., Shoemaker, R.H., Paull, K.D., Monks, A., Tierney, S., Nofziger, T.H., Currens, M.J., Seniff, D., Boyd, M.R., 1988. Evaluation of a soluble tetrazolium/formazan assay for cell growth and drug sensitivity in culture using human and other tumor cell lines. Cancer Res. 48.

Shi, C., Wang, X., Sun, Q., Chen, L., Guan, J., He, L., Zhang, Y., Xu, Y., Cao, J., Chai, Z., Wang, S., Diwu, J., 2022. Decorporation of uranyl in kidneys using an engineered nanocomposite. Environ. Sci. Nano 9, 2704–2712. https://doi.org/10.1039/d2en00133k.

Smedley, P.L., Kinniburgh, D.G., 2023. Uranium in natural waters and the environment: distribution, speciation and impact. Appl. Geochem. 148, 105534 https://doi.org/10.1016/j.apgeochem.2022.105534.

Smith, R.M., Martell, A.E., 1987. Critical stability constants, enthalpies and entropies for the formation of metal complexes of aminopolycarboxylic acids and carboxylic acids. Sci. Total Environ. 64, 125–147. https://doi.org/10.1016/0048-9697(87)90127-6.

Stadler, J., Vogel, M., Steudtner, R., Drobot, B., Kogiomtzidis, A.L., Weiss, M., Walther, C., 2023. The chemical journey of europium(III) through winter rye (Secale cereale L.) – understanding through mass spectrometry and chemical microscopy. Chemosphere 313. https://doi.org/10.1016/j.chemosphere.2022.137252.

Steudtner, R., Arnold, T., Geipel, G., Bernhard, G., 2010. Fluorescence spectroscopic study on complexation of uranium(VI) by glucose: a comparison of room and low temperature measurements. J. Radioanal. Nucl. Chem. 284, 421–429. https://doi.org/10.1007/S10967-010-0489-5.

Steudtner, R., Sachs, S., Schmeide, K., Brendler, V., Bernhard, G., 2011. Ternary uranium (VI) carbonato humate complex studied by cryo-TRLFS. Radiochim. Acta 99, 687–692. https://doi.org/10.1524/ract.2011.1861.

Thiébault, C., Carrière, M., Milgram, S., Simon, A., Avoscan, L., Gouget, B., 2007. Uranium induces apoptosis and is genotoxic to normal rat kidney (NRK-52E) proximal cells. Toxicol. Sci. 98, 479–487. https://doi.org/10.1093/toxsci/kfm130.

Tymen, H., Gerasimo, P., Hoffschir, D., 2000. Contamination and decontamination of rat and human skin with plutonium and uranium, studied with a Franz's chamber. Int. J. Radiat. Biol. 76, 1417–1424. https://doi.org/10.1080/09553000050151709.

Vande Walle, L., Lamkanfi, M., 2016. Pyroptosis. Curr. Biol. 26, R568–R572. https://doi.org/10.1016/j.cub.2016.02.019.

Vanden Berghe, T., Vanlangenakker, N., Parthoens, E., Deckers, W., Devos, M., Festjens, N., Guerin, C.J., Brunk, U.T., Declercq, W., Vandenabeele, P., 2010. Necroptosis, necrosis and secondary necrosis converge on similar cellular disintegration features. Cell Death Differ. 17, 922–930. https://doi.org/10.1038/cdd.2009.184.

Vogel, M., Steudtner, R., Fankhänel, T., Raff, J., Drobot, B., 2021. Spatially resolved Eu (III) environments by chemical microscopy. Analyst 146, 6741–6745. https://doi.org/10.1039/d1an01449h.

Vogler, S., Grosche, A., Pannicke, T., Ulbricht, E., Wiedemann, P., Reichenbach, A., Bringmann, A., 2013. Hypoosmotic and glutamate-induced swelling of bipolar cells in the rat retina: comparison with swelling of Müller glial cells. J. Neurochem. 126, 372–381. https://doi.org/10.1111/jnc.12307.

Wang, E., Taylor, R.W., Pfeiffer, D.R., 1998. Mechanism and specificity of lanthanide series cation transport by ionophores A23187, 4-BrA23187, and ionomycin. Biophys. J. 75, 1244–1254. https://doi.org/10.1016/S0006-3495(98)74044-5.

Wang, K., Li, R., Cheng, Y., Zhu, B., 1999. Lanthanides - the future drugs? Coord. Chem. Rev. 190–192, 297–308. https://doi.org/10.1016/S0010-8545(99)00072-7.

Wang, J., Liu, J., Li, H., Song, G., Chen, Y., Xiao, T., Qi, J., Zhu, L., 2012. Surface water contamination by uranium mining/milling activities in northern Guangdong Province, China. Clean (Weinh) 40, 1357–1363. https://doi.org/10.1002/clen.201100512.

Wang, Y., Gao, W., Shi, X., Ding, J., Liu, W., He, H., Wang, K., Shao, F., 2017. Chemotherapy drugs induce pyroptosis through caspase-3 cleavage of a gasdermin. Nature 547, 99–103. https://doi.org/10.1038/nature22393.

Wang, X., Dai, X., Shi, C., Wan, J., Silver, M.A., Zhang, L., Chen, L., Yi, X., Chen, B., Zhang, D., Yang, K., Diwu, J., Wang, J., Xu, Y., Zhou, R., Chai, Z., Wang, S., 2019. A 3,2-Hydroxypyridinone-based decorporation agent that removes uranium from bones in vivo. Nat. Commun. 10, 1–13. https://doi.org/10.1038/s41467-019-10276-z.

Wang, X., Shi, C., Gao, M., Xu, Y., Jiao, Y., Wan, J., Cao, J., Chai, Z., Diwu, J., 2020. Study of the decorporation efficacy and toxicity of tetradentate 3-hydroxy-2-pyridinone ligands at the cellular level. Radiat. Med. Prot. 1, 159–165. https://doi.org/10.1016/j.radmp.2020.11.006.

Wang, S., Liu, Y., Zhang, L., Sun, Z., 2022. Methods for monitoring cancer cell pyroptosis. Cancer Biol. Med. 19, 398–414. https://doi.org/10.20892/j.issn.2095-3941.2021.0504.

Wetherill, S.F., Guarino, M.J., Cox, R.W., 1981. Acute renal failure associated with barium chloride poisoning. Ann. Intern. Med. 95, 187–188. https://doi.org/10.7326/0003-4819-95-2-187.

Wollenberg, A., Kretzschmar, J., Drobot, B., Hübner, R., Freitag, L., Lehmann, F., Günther, A., Stumpf, T., Raff, J., 2021. Uranium(VI) bioassociation by different fungi – a comparative study into molecular processes. J. Hazard. Mater. 411 https://doi.org/10.1016/j.jhazmat.2021.125068.

Wu, J., Yang, J., Liu, Q., Wu, S., Ma, H., Cai, Y., 2013. Lanthanum induced primary neuronal apoptosis through mitochondrial dysfunction modulated by Ca^{2+} and Bcl-2 family. Biol. Trace Elem. Res. 152, 125–134. https://doi.org/10.1007/s12011-013-9601-3.

Yu, P., Zhang, X., Liu, N., Tang, L., Peng, C., Chen, X., 2021. Pyroptosis: mechanisms and diseases. Signal Transduct. Target. Ther. 6 https://doi.org/10.1038/s41392-021-00507-5.

Yuan, Y., Zheng, J., Zhao, T., Tang, X., Hu, N., 2016. Uranium-induced rat kidney cell cytotoxicity is mediated by decreased endogenous hydrogen sulfide (H2S) generation involved in reduced Nrf2 levels. Toxicol. Res. (Camb). 5, 660–673. https://doi.org/10.1039/c5tx00432b.

Zhang, Y., Shao, X., Kong, X., Yin, L., Wang, C., Lin, L., Ji, Y., 2022. Determination of thorium in the hair and urine of workers and the public in a rare earth mining area. Radiat. Med. Prot. 3, 91–95. https://doi.org/10.1016/j.radmp.2022.03.001.

Zheng, J., Hu, Q., Zou, X., Xu, G., Cao, Y., 2022. Uranium induces kidney cells pyroptosis in culture involved in ROS/NLRP3/caspase-1 signaling. Free Radic. Res. 56, 40–52. https://doi.org/10.1080/10715762.2022.2032021.

Zhivotovsky, B., 2004. Apoptosis, necrosis and between. Cell Cycle 3, 63–65. https://doi.org/10.4161/cc.3.1.606.